THE GEOLOGICAL SOCIETY OF AMERICA®

Holocene volcanism of the upper McKenzie River catchment, central Oregon Cascades, USA

Natalia I. Deligne[1,†], Richard M. Conrey[2,§], Katharine V. Cashman[1,#], Duane E. Champion[3], and William H. Amidon[4]

[1]*Department of Geological Sciences, 1272 University of Oregon, Eugene, Oregon 97403, USA*
[2]*School of the Environment, Washington State University, Box 642812, Pullman, Washington 99164, USA*
[3]*U.S. Geological Survey, Volcano Science Center, MS 910, 345 Middlefield Road, Menlo Park, California 94025, USA*
[4]*Geology Department, Middlebury College, McCardell Bicentennial Hall, Middlebury, Vermont 05753, USA*

ABSTRACT

To assess the complexity of eruptive activity within mafic volcanic fields, we present a detailed geologic investigation of Holocene volcanism in the upper McKenzie River catchment in the central Oregon Cascades, United States. We focus on the Sand Mountain volcanic field, which covers 76 km^2 and consists of 23 vents, associated tephra deposits, and lava fields. We find that the Sand Mountain volcanic field was active for a few decades around 3 ka and involved at least 13 eruptive units. Despite the small total volume erupted (~1 km^3 dense rock equivalent [DRE]), Sand Mountain volcanic field lava geochemistry indicates that erupted magmas were derived from at least two, and likely three, different magma sources. Single units erupted from one or more vents, and field data provide evidence of both vent migration and reoccupation. Overall, our study shows that mafic volcanism was clustered in space and time, involved both explosive and effusive behavior, and tapped several magma sources. These observations provide important insights on possible future hazards from mafic volcanism in the central Oregon Cascades.

INTRODUCTION

Small mafic volcanoes are the most common volcanic landform on Earth; they are found in volcanic fields or on the flanks of larger volcanoes (Valentine and Connor, 2015; de Silva and Lindsay, 2015). Traditionally, small mafic volcanoes have been considered monogenetic, i.e., corresponding to a single batch of magma that erupts only once (e.g., Wood, 1979). More recently, this assumption has been challenged by compositional data that indicate multiple magma sources at single cones (e.g., Brenna et al., 2010; Clynne and Muffler, 2010; Kereszturi et al., 2010; Needham et al., 2011; McGee et al., 2012; Rasoazanamparany et al., 2015). Within volcanic fields, there is often temporally clustered activity (e.g., Condit and Connor, 1996; Kereszturi et al., 2011), and tectonic influences or preexisting structures may control vent locations (e.g., Le Corvec et al., 2013a). Numerous workers have studied the spatial, temporal, volumetric, and geochemical patterns of mafic volcanism in volcanic fields (e.g., Hasenaka and Carmichael, 1985; Kuntz et al., 1986; Conway et al., 1997; Valentine and Perry, 2007; Bebbington and Cronin, 2011; Cebriá et al., 2011; Guilbaud et al., 2011; Le Corvec et al., 2013b). There have also been detailed investigations of select volcanoes within volcanic fields (e.g., Pioli et al., 2008; Rowland et al., 2009; Németh et al., 2012), and studies of associated hazards (e.g., Valentine and Gregg, 2008; Brand et al., 2014). Missing from the literature, however, is a comprehensive mapping investigation of mafic volcanic activity that is clustered in both space and time, despite the potential importance of clustering in volcanic hazard assessment, as well as insights that clustering can provide into the geometry of subvolcanic plumbing systems.

To address the question of clustered volcanism, we present a detailed mapping and preliminary geochemical investigation of mafic volcanic units in the upper McKenzie River catchment in the central Oregon Cascades, United States, focusing on a spatial and temporal cluster of monogenetic cones (Hildreth, 2007) and associated lava fields. This cluster is the 76 km^2 Sand Mountain volcanic field (Sherrod et al., 2004), which consists of the Sand Mountain chain of cones, Nash and Little Nash Craters, the Lost Lake chain of cones, and associated lavas and tephra blankets (Fig. 1). All activity in the upper McKenzie River catchment postdates the ca. 7700 calendar (cal) yr B.P. cataclysmic Mount Mazama eruption (Stuiver et al., 1998; Bacon, 2008), making this one of the youngest volcanic areas in the Cascade Range (Sherrod et al., 2004). The catchment was first investigated by Stearns (1929), with early reconnaissance mapping by Williams (1957). Further mapping by Taylor (1965) identified nine lava units emanating from multiple vent systems in the Sand Mountain volcanic field, along with a "late-stage" unit from Belknap volcano in the upper McKenzie River catchment. The current U.S. Geological Survey (USGS) geologic map (Sherrod et al., 2004) is primarily based on Taylor's work. The concentration of volcanic activity in Sand Mountain volcanic field, both spatially and temporally, provides a unique opportunity to explore concurrent mafic volcanism, vent location, migration, and reoccupation, magma source heterogeneity, and the influence of earlier volcanism on later activity. Importantly, this work provides new insight into potential impacts of future clustered mafic volcanism in the central Oregon Cascades.

BACKGROUND

Geological Setting and Geography of the Upper McKenzie River Catchment

Holocene volcanism in the upper McKenzie River catchment within the High Cascades graben (central Oregon Cascades) is concentrated along the northwestern margin of the graben, close to the boundary between the High and Western Cascades (Fig. 1). The Cascades Range extends from northern California, United States,

[†]Present address: GNS Science, P.O. Box 30368, Lower Hutt 5040, New Zealand; N.Deligne@gns.cri.nz.
[§]Present address: Department of Geosciences, 198 College Hill Road, Hamilton College, Clinton, New York 13323, USA.
[#]Present address: Department of Earth Sciences, University of Bristol, Wills Memorial Building, Queen's Road, Clifton, Bristol, BS8 1RJ, UK.

GSA Bulletin; November/December 2016; v. 128; no. 11/12; p. 1618–1635; doi: 10.1130/B31405.1; 6 figures; 7 tables; Data Repository item 2016130; published online 11 May 2016.

For permission to copy, contact editing@geosociety.org
© 2016 Geological Society of America

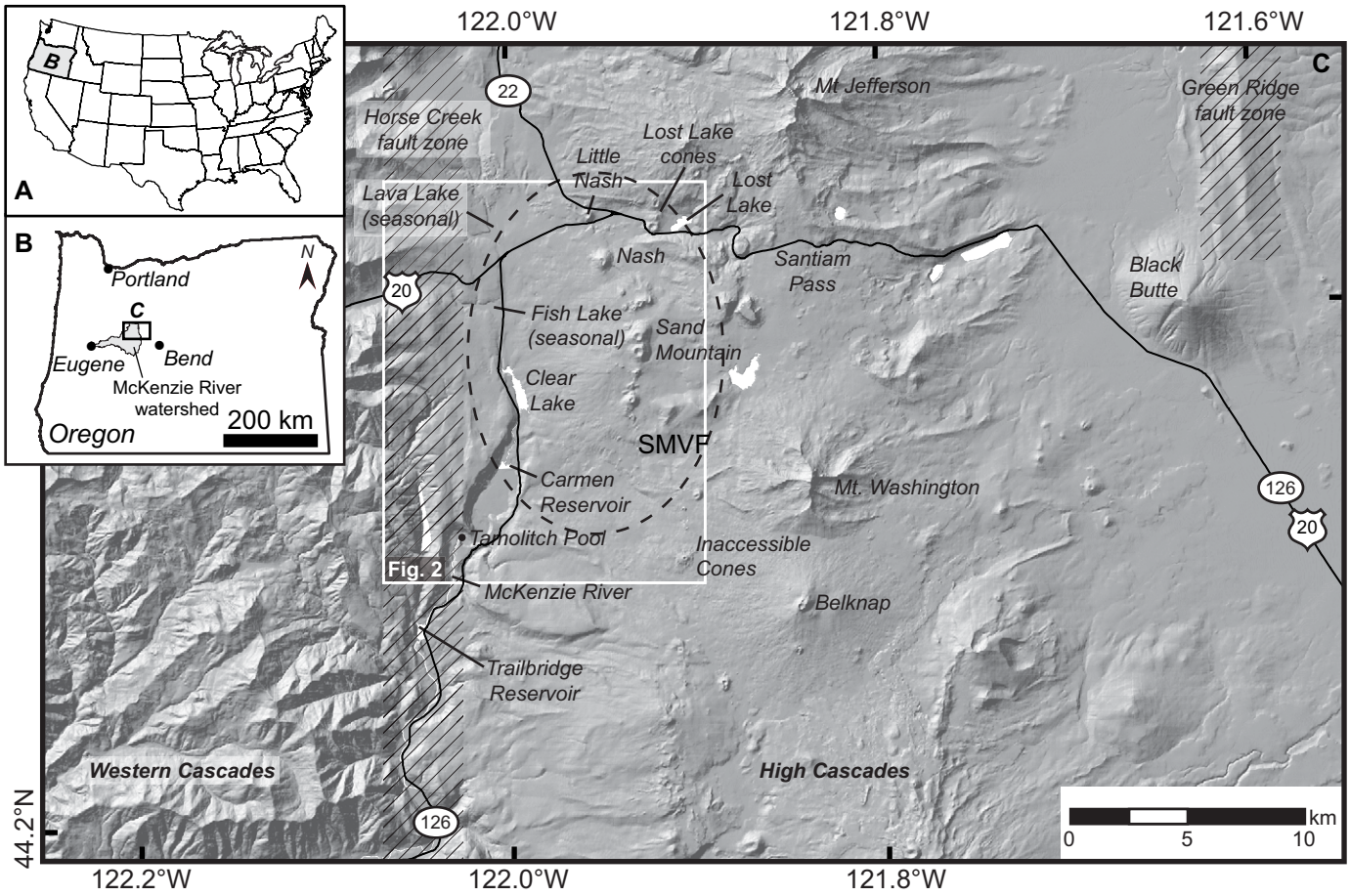

Figure 1. Location maps for the upper McKenzie River catchment. (A) Map of the contiguous United States, with the state of Oregon in gray. (B) Map of Oregon showing the extent of part C with a black rectangle and the McKenzie River watershed in gray. (C) Hillshade of northern portion of central Oregon Cascades, showing labels of geographic features mentioned in text. Sand Mountain volcanic field (SMVF) is within the dashed oval. Central Oregon Cascades graben bounding fault zones are indicated by hashed lines, surface water (year-round lakes and the McKenzie River) is shown in white, and state highways are shown in black.

to southern Canada and results from subduction of the Juan de Fuca plate underneath the North American plate. The central Oregon Cascades range consists of two adjacent volcanic chains: the Western Cascades, which was the axis of volcanism from ca. 35 to 5 Ma, and the High Cascades, which has been the axis of volcanism since ca. 5 Ma (Taylor, 1968; Walker and MacLeod, 1991). This shift in volcanism reflects clockwise rotation of the North American plate over the subduction zone, which has created an apparent eastward migration of volcanism in the central Oregon Cascades and westward migration in the northern Cascades (Wells et al., 1998; McCaffrey et al., 2007; Wells and McCaffrey, 2013). The Western and High Cascades have remarkably different geomorphic expressions: The Western Cascades are highly dissected with a well-developed stream network, whereas the High Cascades are undissected with little to no channel development (Fig. 1). The High Cascades and higher-elevation parts of the Western Cascades were glaciated during the Pleistocene; Pleistocene and older units have large-scale glacial striations and display glacially carved cirques and valleys; evidence of syneruptive lava-ice interactions in the form of Pleistocene tuyas (Sherrod et al., 2004) is also present.

The High Cascades graben is bounded by the Horse Creek fault zone to the west and the Green Ridge fault zone to the east (Fig. 1). The graben is 30 km wide and ~2–3 km deep and is filled by lava (Taylor, 1990; Sherrod et al., 2004). It is a reflection of both Basin and Range extension of the southwestern United States (Sherrod and Smith, 1990) and, probably, clockwise rotation of the North American plate. This graben has been the focus of considerable mafic volcanism, with ~60 km^3 of mafic magma erupted in the past 15 ka, and most of the mapped Quaternary vents (1054 in total) are scoria cones and mafic vents (Hildreth, 2007). As discussed in Schmidt et al. (2008), volcanism within the High Cascades graben forms a distinct geochemical segment of the Cascades arc ("Central segment"), driven by extension and high heat flux. This segment is characterized by an abundance of low-K tholeiites and a more-enriched mantle source than the Columbia segment to the north. Our study area is on the boundary between the Central and Columbia segments of the Cascade arc.

The upper McKenzie River catchment is southwest of Mount Jefferson and northwest of Mount Washington and Belknap volcanoes (Fig. 1). It is within the Willamette National Forest McKenzie Ranger District, and it is an important recreational area—the catchment includes Clear Lake and Tamolitch Pool, which are popular visitor destinations. The upper McKenzie River also hosts the Carmen Smith Hydroelectric Power Scheme, which generates ≤115 kW of electricity. Within the catchment, the Sand Mountain volcanic field is situated close to Santiam Pass, which hosts a ski resort and is one of three passes that cross the central Oregon Cascades. The Sand Mountain volcanic field is

bordered by an important transportation corridor that connects central Oregon with the Willamette Valley. Future volcanism in this area could therefore have substantial societal consequences.

Published Ages

Several ^{14}C ages have been published for upper McKenzie River catchment volcanism (Table 1), and these indicate that the Sand Mountain volcanic field was active at ca. 3 ka. Additionally, two ^{14}C dates (of the same sample) yielded an age of ca. 1.5 ka for the late-stage Belknap unit south of the Sand Mountain volcanic field (Table 1); this unit was mapped by both Taylor (1965) and Sherrod et al. (2004) as entering the McKenzie River valley south of Carmen Reservoir and surrounding Tamolitch Pool.

Tephra Deposit

Our map and sample collection focused solely on the lava fields and vents of the Sand Mountain volcanic field, as well as lavas in the upper McKenzie River catchment. The reader is referred to Mckay (2012) for treatment of associated Sand Mountain volcanic field tephra fall deposits that extend to the east, undertaken as part of a larger project on regional young mafic explosive volcanism. Mckay (2012) mapped the thickness and extent of the entire Sand Mountain volcanic field tephra deposit, which covers ~154 km^2 and has a volume of ~0.39 km^3. While Mckay (2012) noted hundreds of interbedded layers within a relatively continuous deposit, she did not undertake detailed geochemistry to fingerprint individual units. Sand Mountain volcanic field tephra is distinctive due to its remarkable uniformity (mode grain size 125 μm to 0.5 mm) and absence of lapilli, which suggests a hydromagmatic source via interaction with groundwater (Mckay, 2012). No pyroclastic density current deposits have been identified.

METHODS

Geologic Mapping and Geochemical Analyses

The field work presented here was started in the mid-1990s by R.M. Conrey and focused on lava unit identification and general Sand Mountain volcanic field characterization. In 2008, the Eugene Water and Electric Board and Oregon's Department of Geology and Mineral Industries acquired 1-m-resolution research-grade light detection and ranging (LiDAR) data for the McKenzie River. The improved topographic resolution provided by LiDAR in this heavily forested region prompted us to undertake detailed mapping of the southern Sand Mountain volcanic field. We used LiDAR data to identify likely unit extents, presumed unit contacts, and locations for field checking and sample collection; we then mapped several unit contacts in the field using a handheld global positioning system (GPS) device.

We define a unit as a cone and/or lava of similar geochemical composition that is distinct from other units. Mapped lavas were assigned to eruptive units on the basis of the geochemistry of collected samples, as well as field observations of morphology and phenocryst content. Geochemistry was important because many of the lavas are aphyric. Major- and trace-element concentrations were measured by X-ray fluorescence spectroscopy (XRF) at Washington State

TABLE 1. SUMMARY OF AVAILABLE ^{14}C DATES FOR THE SAND MOUNTAIN VOLCANIC FIELD AND THE BELKNAP LAVAS

Sample name	Lab number	Uncalibrated age (1σ)	Calibrated age (2σ)*	Description	Reference
TFJ-60A	WSU-370+	1400 ± 100 yr B.P.	(94.7%) 1344 ± 178 cal. yr B.P. (A.D. 427–784) (3.3%) 1143 ± 21 cal. yr B.P. (A.D. 786–828) (2.0%) 1098 ± 13 cal. yr B.P. (A.D. 839–865)	Reanalysis of sample TFJ-60 described below	Champion (1980)
TFJ-60	WSU-292	1590 ± 160 yr B.P.	(99.1%) 1554 ± 318 cal. yr B.P. (A.D. 79–714) (0.9%) 1194 ± 11 cal. yr B.P. (A.D. 745–767)	Charred roots excavated from base of tree mold within the late-stage Belknap lava unit of Taylor (1965) roughly 0.8 km (0.5 mi) east of Highway126	Taylor (1965)
TFJ-204	WSU-371	1950 ± 150 yr B.P.	*(94.3%) 2265 ± 79 cal. yr B.P. (236–394 B.C.)* *(4.9%) 2268 ± 40 cal. yr B.P. (358–278 B.C.)* *(0.8%) 2,00 ± 9 cal. yr B.P. (259–241 B.C.)*	Charred wood underneath cinders from cone immediately southwest of Potato Hill, presumably Jack Pine vent	Chatters (1968)
870804-1	W-6018	2590 ± 150 yr B.P.	(100.0%) 2687 ± 353 cal. yr B.P. (1090–384 B.C.)	Charcoal at contact between soil and tephra attributed to Nash and the northern Sand Mountain volcanic field	Sherrod et al. (2004)
Sample b	N.R.†	2705 ± 200 yr B.P.	(98.2%) 2810 ± 462 cal. yr B.P. (1323–398 B.C.) *(1.8%) 3308 ± 24 cal. yr B.P. (1382–1334 B.C.)*	Outer wood of ~0.3-m-diameter(1-ft-diameter) stump submerged in Clear Lake at depth of 4 m (13 ft), collected in November 1963	Benson (1965)
CL1964	AA-30522	2750 ± 45 yr B.P.	(100.0%) 2856 ± 92 cal. yr B.P. (998–815 B.C.)	Part of 0.3 m "rooted snag" submerged in Clear Lake collected by E.M. Taylor in summer 1964 (Licciardi et al., 1999) near the Cold Water Cove campground boat ramp (E.M. Taylor personal commun. to R.M. Conrey, 1995)	Licciardi et al. (1999)
NID10-16MK	N1D10-16MK	2870 ± 20 yr B.P.	(100.0%) 3000 ± 73 cal. yr B.P. (1123–977 B.C.)	Outer wood of tree submerged in Clear Lake at depth of 40 m (130 ft) near UTM 10N E0580112 N4912933 (WGS1984)	Deligne et al. (2013)
TFJ-213	WSU-449	2990 ± 300 yr B.P.	(98.9%) 3144 ± 716 cal. yr B.P. (1910–479 B.C.) *(1.1%) 2392 ± 28 cal. yr B.P. (470–414 B.C.)*	Charred roots beneath lava on east side of Clear Lake	Champion (1980)
Sample a	N.R.†	3200 ± 220 yr B.P.	(99.5%) 3394 ± 536 cal. yr B.P. (1981–908 B.C.) *(0.5%) 3956 ± 11 cal. yr B.P. (2017–1995 B.C.)*	Inner wood of sample b described above	Benson (1965)
TFJ-205	WSU-372	3850 ± 215 yr B.P.	(100.0%) 4270 ± 566 cal. yr B.P. (2884–1756 B.C.)	Charred root bark surrounded by soil and roots found near Old Santiam Wagon Road, described as dating the Fish Lake lava unit of Taylor (1968), referred to as the Hackleman Creek lava flow in Champion (1980)	Chatters (1968)

Note: ^{14}C dates inconsistent with stratigraphic relations and/or other dating methods presented in this study are *italicized* and are included for completeness; for more detailed discussion of these ages, see Sherrod et al. (2004).

*Calibrated age determined with Calib Rev 6.1.0, using calibration curve IntCal 09 (Stuiver et al., 2005; Reimer et al., 2009).

†N.R.—not reported.

University, Pullman (Table DR1[1]). Samples include lava (319 samples), scoria and agglutinate collected at or near vents (13 samples), and bombs (28 samples); we collected fresh black unaltered samples when possible. We located samples on either a 7.5 min quadrant or (starting in 2002) with a handheld GPS device (Table DR2 [see footnote 1]). Device location errors for samples collected in 2009 and later are generally <10 m. We assigned vents to eruptive units solely on the basis of geochemistry.

A final geologic map was produced in ArcMap 10.2.2; contacts were drawn at 1:2500 scale in regions with LiDAR data and 1:10,000 scale elsewhere. Walked contacts were traced at 1:750, assuming a 6 m possible location error and (where LiDAR data exist) accounting for aspect and flow front consistency. Where LiDAR data were not available, notably in the vent areas and in the northern Sand Mountain volcanic field, we used a combination of a 10 m digital elevation model (DEM)–derived hillshade map and 0.5 m pixel georeferenced aerial photography (available from Oregon Image Explorer, http://oregonexplorer.info/) to inform unit contact placement. For this reason, and given the limited amount of time spent in the northern Sand Mountain volcanic field, we stress that contacts in areas without LiDAR coverage are approximately located, and thus mapping of the northern Sand Mountain volcanic field should be treated as reconnaissance.

Relative and Quantitative Dating

We used both relative and quantitative dating techniques to establish eruption chronology. Relative ages were established at observed field contacts or inferred from unit extents such that continuous lava units were assumed to be younger than adjacent discontinuous units. We used three quantitative dating techniques for single units: existing ^{14}C ages (Table 1), analysis of paleomagnetic secular variation, and cosmogenic ^{3}He surface exposure dating (see supplementary file for detailed methods [footnote 1]).

Paleomagnetic samples were collected, processed, and interpreted using the methods described in McElhinny (1973). Cosmogenic ^{3}He surface exposure dating measures the ^{3}He concentration of olivine grains collected within <4 cm of the surface (Cerling, 1990); olivine grains were prepared following the procedure in Amidon and Farley (2011). We used Licciardi et al.'s (1999) calibrated production rate for the Sand Mountain volcanic field for each site using the method of Desilets et al. (2006). We collected samples for XRF analysis at or within 100 m of each paleomagnetic and cosmogenic sample site to confirm eruptive unit assignment.

Erupted Volumes

Erupted volumes for single lava units were calculated assuming a uniform lava flow thickness of 10 m, consistent with field observations. Lava units with discontinuous exposure were conservatively reconstructed to form one lava unit, without covering exposed stratigraphically younger units. Scoria cone volumes were crudely estimated using the formula for a cone with equivalent circle radii for the given cone footprint; we did not account for the volume excavated by the vent. We estimated lava dense rock equivalent (DRE) by assuming that lava density is equal to magma density, and scoria cone DRE by assuming scoria cone material density of 1500 kg/m^3 (McGetchin et al., 1974) and magma density of 2500 kg/m^3 (Crosweller et al., 2012).

RESULTS

Sand Mountain volcanic field lavas and 23 associated identifiable cones cover 76 km^2. We identified three main geochemical groups within the Sand Mountain volcanic field: the Sand, Nash, and Lost Lake groups. The three groups contain a total of 13 eruptive units, including three "orphan" lavas (no presently exposed associated vents) and one line of cones without associated lavas. A unit could include multiple lavas from different vents. We mapped the southern Sand Mountain volcanic field (Sand group, covered by LiDAR data) in detail, and the northern Sand Mountain volcanic field (Nash and Lost Lake groups; Fig. 2) in a more reconnaissance fashion. All assigned names are informal; for geographic features and places, we use official place names unless explicitly stated otherwise.

The Sand group consists of five eruptive units—Clear Lake South, Clear Lake South A, Ice Cap, Great Spring, and Clear Lake East—and includes one line of cones without associated lava (Clear Lake South A). Farther north, the Nash group consists of four eruptive units (Early Nash I, Early Nash II, Nash, and Little Nash) and includes two orphan lava units (Early Nash I and II), that is, lavas without identifiable vents. The Lost Lake group consists of four eruptive units (Cold Water Cove, Fish Lake, Old Wagon Road, and Lost Lake), with one orphan lava unit (Cold Water Cove).

Within the Sand Mountain volcanic field, near the Lost Lake group, there is an isolated cone without associated lava (Jack Pine cone), and lava with limited exposure and no associated vent (SnoPark lava unit); both lie in a small area between the Nash and Lost Lake groups. South of the Sand Mountain volcanic field, there are two lava units (Tamolitch and Belknap) that entered the McKenzie River valley but were sourced at or near Belknap volcano and the Inaccessible chain of cones; we present detailed mapping and stratigraphic relations of these lavas where LiDAR data are available within the upper McKenzie River catchment.

Petrologic Observations

Petrologic descriptions based on hand sample and thin-section observations of lava units mapped in detail (i.e., Sand group lavas and Cold Water Cove [Lost Lake group], Tamolitch and Belknap lavas) are provided in Table 2. Within the Sand group, Clear Lake East lava is easily distinguishable by the abundance of plagioclase microphenocrysts, which are absent in the other Sand group lavas. Differences among the other Sand group lavas are more subtle, although Clear Lake South lava typically has large (<4 mm) olivine crystals. Within the Lost Lake group, Lost Lake lava has large (typically ~3 mm, but up to 7 mm) olivine crystals, with olivine abundances ≤5%. Fish Lake lava has groundmass plagioclase and ~1% large (<4 mm) olivine crystals. Plagioclase is absent from Old Wagon Road lava, which has a bimodal size distribution of olivine crystals (~0.5 mm or 2–3 mm). Within the Nash group, Early Nash I and II lavas have more olivine than Nash and Little Nash lavas. South of the Sand Mountain volcanic field, the Tamolitch and Belknap lavas can be distinguished by the abundance of plagioclase and olivine crystals in Tamolitch lava relative to aphyric Belknap lava.

Geochemistry

Sand Mountain volcanic field lavas are calc-alkaline basalt, basaltic andesite, and alkaline basalt (Fig. 3). Unlike some other young lava in the region (e.g., Deardorff and Cashman, 2012), single units have homogeneous compositions, which we used to identify eruptive units (Fig. 3; Table DR1 [see footnote 1]). Distinguishing elements are SiO_2, TiO_2, MgO, and CaO (major elements, wt%; Table 3), and Ni, Sr, and Ba (trace elements, ppm; Table 4).

The Sand group shows the greatest variation in composition and ranges from basalt to basaltic andesite. Single Sand group units are distinguishable from each other on the basis of SiO_2, TiO_2, Sr, and Ba concentrations (Fig. 3).

[1]GSA Data Repository item 2016130, detailed quantitative dating method explanation, sample major- and trace-element concentrations measured by X-ray fluorescence spectroscopy (XRF; Table DR1), and sample location and collection details (Table DR2), is available at http://www.geosociety.org/pubs/ft2016.htm or by request to editing@geosociety.org.

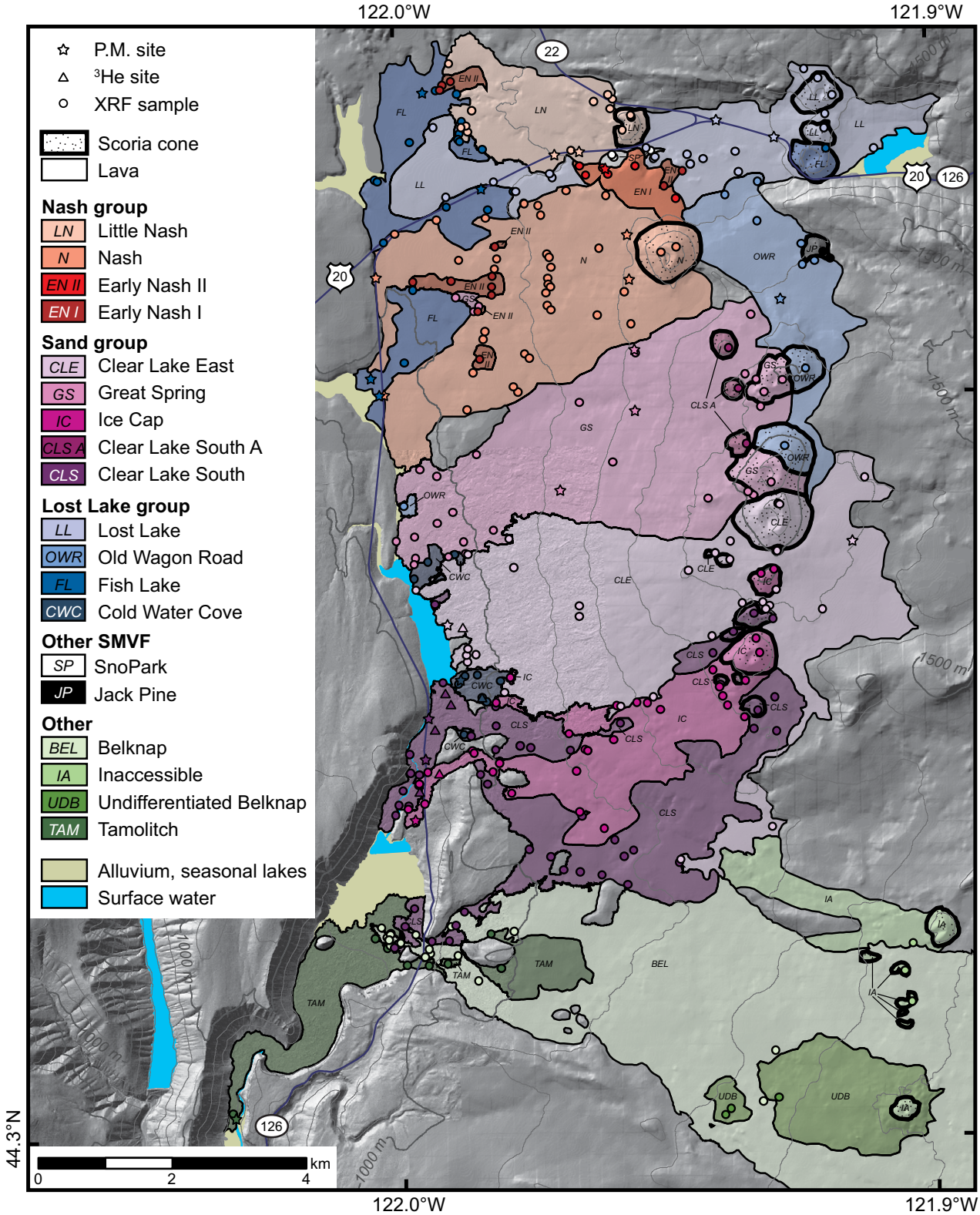

Figure 2. Geologic map of the Sand Mountain volcanic field and other Holocene lavas of the upper McKenzie River catchment. Lava units are outlined, and scoria cones are outlined in bold and stippled. Tephra fall deposits are not shown (see Mckay, 2012). Base map is a shaded relief map constructed from light detection and ranging (LiDAR) data where available and a 10 m digital elevation model elsewhere. Paleomagnetic (P.M., stars), ^{3}He (triangles), and X-ray fluorescence (XRF; circles) sample locations are shown; note that XRF samples were also collected at paleomagnetic and ^{3}He sites. Also shown are key highways (black lines) and 100 m contour intervals (gray, with bold 500 m contour intervals). Refer to Figure 1C for geographic names.

TABLE 2. PETROGRAPHIC DESCRIPTIONS OF LAVA MAPPED IN DETAIL

Eruptive unit	Phenocrysts	Groundmass
SAND GROUP		
Clear Lake East	10%–15% plagioclase, 2% olivine Plagioclase: mostly laths, up to 2 mm long Olivine: generally 1 mm diameter, some glomerocrysts	Microcrystalline plagioclase and olivine
Great Spring	5% olivine, <1.5% plagioclase Olivine: generally ≤1 mm, can be up to 3 mm diameter Plagioclase: mostly laths, small	Highly microcrystalline plagioclase and olivine
Ice Cap	3% olivine, <1% plagioclase Olivine: generally ≤2 mm, can be up to 3 mm diameter Plagioclase: generally equant (few laths) Large glomerocrysts of olivine and plagioclase	Microcrystalline plagioclase and olivine
Clear Lake South	7% olivine, <0.1% plagioclase Olivine: bimodal size distribution, with submillimeter and 1–4-mm-diameter grains; larger grains typically >2 mm	Microcrystalline plagioclase (abundant) and olivine
LOST LAKE GROUP		
Cold Water Cove	5% olivine, trace plagioclase Olivine: bimodal size distribution, with submillimeter and 1–2-mm-diameter grains	Highly microcrystalline plagioclase and olivine
OTHER		
Belknap	1% olivine, trace plagioclase Olivine: generally ≤1 mm, can be up to 4 mm diameter (rare) Overall few phenocrysts Very glassy and vesicular	Very glassy
Tamolitch	10% plagioclase, 5% olivine Plagioclase: up to 2 mm diameter Olivine: ≤1 mm diameter Glomerocrysts of olivine and plagioclase common	Very crystalline, although glass visible

Clear Lake East lavas are the most evolved, with the highest SiO_2, Ba, and Sr and lowest TiO_2. Clear Lake South lavas are the least evolved, with low SiO_2, Ba, and Sr and anomalously high TiO_2.

The Nash group is entirely basaltic andesite, and single units are homogeneous in composition. The Nash group can be distinguished from the other groups not only by high SiO_2 content, but also by high FeO/MgO ratio, low MgO, TiO_2, CaO, and Cr concentrations, and different Ni versus MgO trends. Single units show differences in SiO_2, MgO, Ni, and Sr concentrations.

The Lost Lake group is mostly basalt, and single units show tight compositional clusters; it differs from the other groups in its high MgO content and relatively low FeO/MgO ratio. Single units show differences in Ba and Sr concentrations; Fish Lake lavas have the lowest Ba and Sr, and the other three units show variations in Ba at similar Sr values, with Lost Lake lavas having the highest Ba. Lost Lake lavas also have the highest K_2O concentrations in the group.

SnoPark lava and Jack Pine cone samples have compositions that are unique in the Sand Mountain volcanic field. SnoPark lava shares some similarities with the Lost Lake group and the Clear Lake South eruptive unit (Sand group), but it is sufficiently different (e.g., higher Ba and K_2O) to preclude inclusion in those units. The Jack Pine cone, in contrast, has a composition that is different from the rest of the Sand Mountain volcanic field in that it is an alkali basalt with exceedingly high Ba (>1000 ppm) and Sr (>1300 ppm) concentrations.

South of the Sand Mountain volcanic field, the Tamolitch and Belknap lavas are low-Sr basalts; the two units are distinguishable on the basis of SiO_2, TiO_2, CaO, and Ba concentrations. Tamolitch and Belknap lavas are, respectively, less and more evolved. Three samples from within mapped Belknap (NID10-26MK) and Tamolitch (NID10-27MK and NID10-29MK) lavas have similar SiO_2 and Sr values but are otherwise chemically different from these two eruptive units; we refer to these three samples as "undifferentiated Belknap." We have not identified the source of the Tamolitch lavas.

Lava Physical Characteristics

Sand Mountain volcanic field lavas are broadly characterized by blocky lava morphologies, although limited parts of the Fish Lake lavas (Lost Lake group) have pāhaoehoe ropes. Lava flow fronts are ≤15 m thick in the Ice Cap (Sand group), Fish Lake, Lost Lake, and Cold Water Cove (Lost Lake group) lavas. The LiDAR data also highlight a pronounced levee system (20 m of relief) within Cold Water Cove lava immediately southeast of Clear Lake (Fig. 2); the exposed portion of the SnoPark lava consists primarily of preserved levees. These observations suggest that during Sand Mountain volcanic field lava flow emplacement, flows were blocky, thick, and, in many places, controlled by levee systems.

The blocky Clear Lake East lavas are unusual in the Sand Mountain volcanic field in that no associated levees have been identified. These lavas were fed, at least in part, by a lava tube system exposed at Lucy's Cavern (44.376°N, 121.946°W). The tube trends S20°E, extends at least ~150 m, and is, in places, ~8–10 m deep; it has remarkable drip features and a vaulted roof that pinches to a narrow elongated top. Additionally, we located the two "vertical pipes" first mentioned by Taylor (1965) at 44.378°N, 121.939°W and 44.378°N, 121.938°W (Nieland's [1970] "Moss" and "Century" pits, respectively), with depths of 19 m and 30 m, respectively (Nieland, 1970). These deep circular pits have an ~1-m-diameter opening situated at the top of two separate mounds. Also unique to the Clear Lake East lavas are centimeter-scale alternating bands of fresh and oxidized lava along most of the margin with Clear Lake.

In contrast to Sand Mountain volcanic field lavas, the Tamolitch and Belknap lavas primarily have submeter flow fronts, well-defined pāhoehoe ropes, and pronounced tumuli characteristic of flow inflation. The Tamolitch lava also contains well-preserved tree molds, some of which were noted by Stearns (1929). During emplacement, these flows were likely much thinner and more fluid than their Sand Mountain volcanic field counterparts.

Age Measurements

Paleomagnetic Constraints

The scatter of Sand Mountain volcanic field paleomagnetic site mean directions on an equal-area diagram (Fig. 4A) is remarkably small. Sites within the Sand, Nash, and Lost Lake groups record a normal polarity remanent direction with mean inclination near 50°, and slightly easterly declinations (Table 5). The similarity among mean directions of the Sand, Nash, and Lost Lake eruptive groups strongly indicates that they are of the same eruptive age and span a time interval no longer than a century. In contrast, results from the Tamolitch basalt are steeper in inclination, and more westerly in declination (Fig. 4B). The Tamolitch paleomagnetic data show that it is not coeval with Sand Mountain volcanic field volcanism; stratigraphic constraints indicate that it is older.

Cosmogenic ^{3}He Exposure Age Dating

We determined cosmogenic ^{3}He exposure ages for seven samples in the vicinity of Clear Lake: one sample each for the Cold Water Cove, Ice Cap, and Great Spring lavas, and four for the Clear Lake South lavas (Table 6). Six of the samples yielded ages between 2.7 and 3.1 ka, with the Clear Lake East and Ice Cap lava ages consistently younger than those of the Clear Lake South and Cold Water Cove lavas. These ages agree with the paleomagnetic data and stratigraphic relations, both in relative age and in field constraints, which suggest lava emplacement over a short period of time.

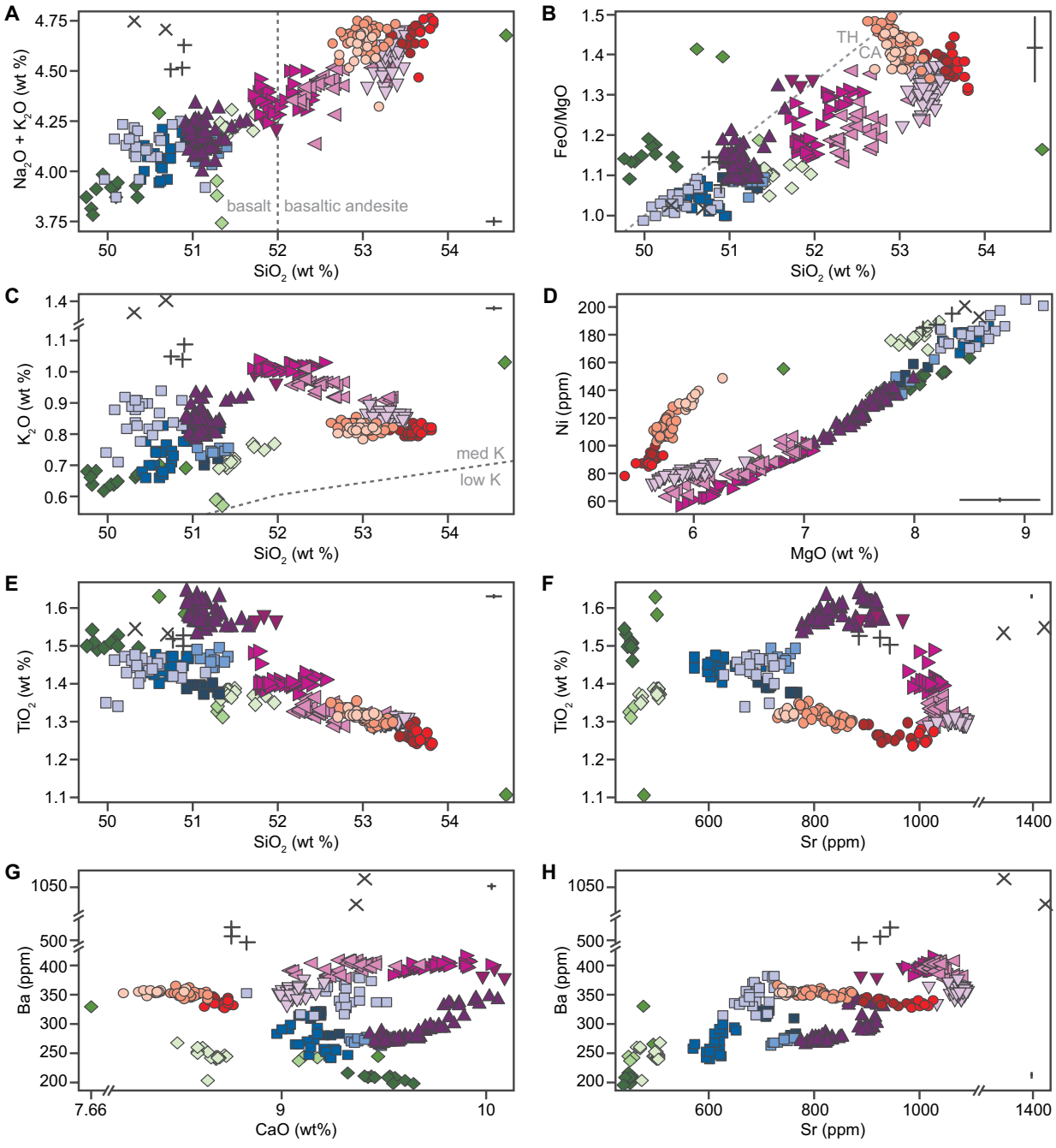

Figure 3. Harker plots for the units mapped in this study; unit colors correspond to Figure 2. Major and minor elements are in weight percent (wt%), and trace elements are in parts per million (ppm); plotted data have been recalculated volatile-free. Compositional ranges are given in Tables 3 and 4, and full analyses are given in Table DR1 (see text footnote 1). X-ray fluorescence (XRF) instrument error bars (2σ) are shown on each plot. (A) $Na_2O + K_2O$ vs. SiO_2, with basalt and basaltic andesite fields shown following Le Bas et al. (1986). (B) FeO/MgO vs. SiO_2, with tholeiitic (TH) and calc-alkaline (CA) fields shown following Arculus (2003). (C) K_2O vs. SiO_2, with low- and medium-K fields shown following Gill (1981). (D) Ni vs. MgO. (E) TiO_2 vs. SiO_2. (F) TiO_2 vs. Sr. (G) Ba vs. CaO. (H) Ba vs. Sr. SMVF—Sand Mountain volcanic field.

The seventh sample, from Clear Lake South lava, has an age of 7.4 ka, which is inconsistent with both stratigraphic relations established at numerous places across the Sand Mountain volcanic field and with internal Clear Lake South lava lobe stratigraphy (i.e., the 7.4 ka lava lobe overlies a ca. 3 ka lava lobe). For this reason, we assume that the date is incorrect.

Stratigraphic Relations

We established stratigraphic relations (Fig. 5) for all contacts within the LiDAR-mapped region on the basis of targeted field observations, and elsewhere though a combination of field observations and map relationships. "Orphan" lavas do not have an exposed vent.

In the Nash group, Early Nash I appears to be the oldest, because it is covered by the other three eruptive units. It, along with Early Nash II, is an orphan lava unit. Early Nash II underlies both Nash and Little Nash, but it surrounds SnoPark levees and is presumably younger. Stratigraphically, it is unclear which of Nash or Little Nash is younger. Nash group lavas overlie Great Spring lavas (Sand group) and the Fish Lake, Old Wagon Road, and Lost Lake lavas (Lost Lake group).

Clear Lake East lavas overlie all other Sand group lavas. Clear Lake South lavas underlie Ice Cap lavas. No contacts are exposed between Great Spring lavas and either the Clear Lake South or Ice Cap lavas, although north of Clear Lake, a small exposure of Old Wagon Road lava (Lost Lake group) underlies Great Spring lavas. West of Fish Lake, a small exposure of Great Spring lava is underneath both Nash and Early Nash II lavas (Nash group) and above Fish Lake lavas (Lost Lake group). The Clear Lake South A vents are surrounded and partially buried by Great Spring lavas.

Differences in soil and associated vegetation cover (Deligne et al., 2013) provide a further clue in deciphering the chronology of the Nash and Sand groups: In the southern Sand Mountain volcanic field, mature forests exist on lavas covered with Sand Mountain volcanic field tephra (Cold Water Cove, Clear Lake South, Ice Cap, and Great Spring lavas), whereas younger lavas without tephra are relatively barren (Nash, Little Nash, and Clear Lake East lavas). Soil on Cold Water Cove, Clear Lake South, and Clear Lake East lavas (the latter in a localized vegetated area near the vent area) consists of one or two tephra layers, but beyond having general geochemical Sand Mountain volcanic field characteristics, tephra layer compositions did not match specific eruptive units (Deligne et al., 2013). Early Nash I and II, Lost Lake group, and SnoPark lavas in the northern Sand Mountain volcanic field also host mature forests. We used these findings to infer that all currently barren Sand Mountain volcanic field lava units postdate Sand Mountain volcanic field explosive activity. Conversely, these observations constrain the timing of the explosive phase of eruptive activity.

In the Lost Lake group, Fish Lake lavas underlie Lost Lake lavas and the Nash group, whereas Old Wagon Road lavas underlie the Great Spring unit (Sand group). Lost Lake lavas underlie the Nash group and surround SnoPark levees and are presumably younger. Due to poor field exposure of contacts and inconclusive map relationships, we could not determine the relation between the Old Wagon Road and Lost Lake lava units. Cold Water Cove lavas underlie all Sand group lavas and have no exposed lava contacts with units from either the Nash or Lost Lake groups. The Jack Pine cone has no associated lava but is over-

TABLE 3. ERUPTIVE UNIT RANGE OF NORMALIZED MAJOR-ELEMENT WEIGHT PERCENT CONCENTRATIONS

Eruptive unit (*N*) Metric	SiO_2	TiO_2	Al_2O_3	FeO	MnO	MgO	CaO	Na_2O	K_2O	P_2O_3
NASH GROUP										
Little Nash (16)										
Min	52.72	1.305	17.61	8.15	0.141	5.88	8.22	3.51	0.78	0.399
Mean	52.98	1.313	17.78	8.40	0.142	5.99	8.38	3.79	0.81	0.404
Max	53.18	1.330	17.89	8.64	0.143	6.27	8.53	3.87	0.83	0.410
Range	0.46	0.025	0.28	0.49	0.003	0.39	0.31	0.36	0.05	0.012
Stdev	0.12	0.006	0.07	0.16	0.001	0.08	0.08	0.09	0.01	0.004
Nash (38)										
Min	52.65	1.278	17.81	7.74	0.135	5.64	8.46	3.73	0.79	0.379
Mean	53.01	1.309	17.97	8.21	0.138	5.75	8.55	3.85	0.82	0.395
Max	53.37	1.347	18.10	8.54	0.142	5.87	8.64	3.92	0.85	0.413
Range	0.72	0.069	0.29	0.80	0.007	0.23	0.18	0.19	0.06	0.035
Stdev	0.17	0.018	0.07	0.18	0.002	0.06	0.05	0.04	0.01	0.010
Early Nash II (8)										
Min	53.64	1.232	17.79	7.40	0.127	5.38	8.62	3.65	0.80	0.350
Mean	53.74	1.251	17.93	7.62	0.129	5.58	8.70	3.88	0.82	0.364
Max	53.83	1.274	18.09	7.81	0.137	5.73	8.76	3.96	0.83	0.395
Range	0.19	0.043	0.30	0.41	0.011	0.35	0.14	0.31	0.03	0.045
Stdev	0.08	0.015	0.11	0.14	0.004	0.10	0.05	0.10	0.01	0.014
Early Nash I (13)										
Min	53.32	1.238	17.75	7.58	0.128	5.54	8.64	3.80	0.79	0.351
Mean	53.54	1.263	17.95	7.74	0.131	5.63	8.70	3.87	0.80	0.362
Max	53.66	1.293	18.07	7.92	0.134	5.68	8.76	3.92	0.83	0.379
Range	0.34	0.055	0.32	0.35	0.007	0.14	0.12	0.12	0.04	0.028
Stdev	0.11	0.019	0.09	0.11	0.002	0.04	0.04	0.04	0.01	0.008
SAND GROUP										
Clear Lake East (40)										
Min	53.04	1.284	17.32	7.47	0.131	5.61	8.98	3.55	0.82	0.377
Mean	53.32	1.295	17.55	7.76	0.134	5.93	9.06	3.71	0.85	0.384
Max	53.52	1.305	17.77	8.00	0.138	6.46	9.20	3.85	0.89	0.392
Range	0.47	0.021	0.45	0.52	0.007	0.85	0.23	0.30	0.06	0.014
Stdev	0.12	0.005	0.12	0.14	0.002	0.18	0.04	0.07	0.01	0.004
Great Spring (33)										
Min	52.17	1.287	17.00	7.51	0.135	5.73	9.03	3.20	0.88	0.372
Mean	52.66	1.321	17.29	7.98	0.142	6.46	9.32	3.50	0.95	0.388
Max	53.34	1.364	17.76	8.28	0.153	7.01	9.67	3.71	1.01	0.416
Range	1.18	0.077	0.76	0.77	0.018	1.29	0.64	0.51	0.13	0.045
Stdev	0.36	0.019	0.20	0.22	0.004	0.41	0.14	0.11	0.03	0.009
Ice Cap (36)										
Min	51.73	1.373	16.96	7.70	0.141	5.89	9.55	3.23	0.97	0.362
Mean	52.05	1.406	17.20	8.09	0.144	6.62	9.74	3.36	1.01	0.376
Max	52.58	1.485	17.53	8.32	0.150	7.09	10.03	3.48	1.04	0.411
Range	0.85	0.112	0.57	0.62	0.009	1.20	0.49	0.25	0.06	0.049
Stdev	0.24	0.023	0.19	0.16	0.002	0.40	0.12	0.06	0.01	0.008
Clear Lake South A (3)*										
RC03-49	51.98	1.561	17.46	8.13	0.146	6.10	10.04	3.24	0.96	0.389
RC03-50	51.84	1.572	17.32	8.19	0.145	6.21	10.09	3.25	1.00	0.378
RC04-25	51.73	1.559	17.31	8.32	0.145	6.24	9.98	3.34	0.99	0.382
Clear Lake South (55)										
Min	50.93	1.537	16.56	8.21	0.145	6.42	9.43	3.20	0.79	0.350
Mean	51.14	1.588	16.81	8.57	0.148	7.53	9.66	3.34	0.84	0.369
Max	51.65	1.647	17.27	8.77	0.152	7.99	10.06	3.47	0.94	0.393
Range	0.73	0.109	0.71	0.57	0.007	1.57	0.63	0.27	0.15	0.043
Stdev	0.14	0.026	0.12	0.12	0.002	0.29	0.16	0.06	0.04	0.009

(*continued*)

TABLE 3. ERUPTIVE UNIT RANGE OF NORMALIZED MAJOR-ELEMENT WEIGHT PERCENT CONCENTRATIONS (*continued*)

Eruptive unit (*N*) Metric	SiO_2	TiO_2	Al_2O_3	FeO	MnO	MgO	CaO	Na_2O	K_2O	P_2O_3
LOST LAKE GROUP										
Lost Lake (24)										
Min	49.98	1.340	16.53	8.63	0.151	8.24	8.82	3.10	0.71	0.324
Mean	50.45	1.437	16.71	8.91	0.154	8.59	9.28	3.27	0.85	0.347
Max	51.16	1.474	16.83	9.09	0.159	9.18	9.51	3.43	0.94	0.359
Range	1.18	0.133	0.30	0.46	0.008	0.94	0.69	0.33	0.22	0.035
Stdev	0.27	0.034	0.07	0.13	0.002	0.23	0.14	0.08	0.06	0.009
Old Wagon Road (10)										
Min	51.05	1.442	16.70	8.48	0.146	7.72	9.33	3.30	0.73	0.336
Mean	51.24	1.465	16.82	8.59	0.149	7.87	9.41	3.36	0.75	0.342
Max	51.41	1.493	16.99	8.84	0.155	8.19	9.51	3.43	0.76	0.354
Range	0.36	0.051	0.29	0.36	0.009	0.47	0.17	0.13	0.03	0.018
Stdev	0.11	0.018	0.08	0.11	0.002	0.14	0.07	0.04	0.01	0.005
Fish Lake (21)										
Min	50.41	1.402	16.60	8.47	0.150	8.26	8.97	3.28	0.66	0.320
Mean	50.65	1.447	16.79	8.87	0.154	8.50	9.15	3.36	0.73	0.341
Max	50.96	1.474	16.94	9.08	0.157	8.68	9.32	3.46	0.83	0.364
Range	0.55	0.072	0.34	0.61	0.007	0.42	0.35	0.18	0.17	0.045
Stdev	0.15	0.019	0.08	0.19	0.002	0.10	0.09	0.05	0.05	0.013
Cold Water Cove (11)										
Min	50.93	1.373	16.91	8.51	0.148	7.76	9.08	3.29	0.70	0.343
Mean	51.15	1.386	17.02	8.69	0.152	7.89	9.20	3.36	0.79	0.361
Max	51.32	1.403	17.14	8.94	0.157	8.12	9.31	3.46	0.83	0.375
Range	0.39	0.030	0.23	0.44	0.009	0.36	0.22	0.17	0.13	0.033
Stdev	0.12	0.011	0.08	0.13	0.003	0.10	0.06	0.05	0.05	0.010
OTHER SAND MOUNTAIN VOLCANIC FIELD										
SnoPark (3)*										
RC03-57	50.89	1.525	16.36	9.17	0.157	8.08	8.82	3.48	1.04	0.480
RC11-11	50.76	1.519	16.25	9.38	0.156	8.20	8.75	3.46	1.05	0.483
RC12-08	50.90	1.501	16.26	8.98	0.155	8.34	8.75	3.54	1.09	0.481
Jack Pine (2)*										
RC04-34	50.70	1.531	15.80	8.63	0.145	8.46	9.40	3.30	1.41	0.618
RC12-06	50.32	1.547	15.81	8.83	0.148	8.60	9.36	3.38	1.37	0.632
OTHER										
Belknap (17)										
Min	51.33	1.346	16.80	8.53	0.148	7.79	8.48	3.43	0.69	0.306
Mean	51.51	1.373	16.94	8.82	0.150	8.02	8.64	3.51	0.72	0.312
Max	51.96	1.386	17.13	8.94	0.151	8.23	8.72	3.60	0.77	0.332
Range	0.63	0.040	0.33	0.41	0.004	0.44	0.24	0.16	0.08	0.026
Stdev	0.18	0.012	0.09	0.11	0.001	0.11	0.06	0.04	0.03	0.007
Inaccessible cones (3)*										
SHE95-TFJ23	51.30	1.325	17.39	8.66	0.160	7.84	9.10	3.36	0.59	0.294
SHE95-TFJ24	51.29	1.340	17.51	8.61	0.161	7.73	9.17	3.29	0.59	0.295
SHE95-TFJ25	51.35	1.311	17.42	9.04	0.159	7.62	9.08	3.17	0.57	0.277
Undifferentiated Belknap (3)*										
NID10-26MK	54.67	1.108	16.74	7.93	0.135	6.81	7.66	3.65	1.03	0.280
NID10-27MK	50.61	1.628	17.52	9.34	0.165	6.61	9.46	3.59	0.70	0.394
NID10-29MK	50.92	1.581	17.59	9.12	0.160	6.54	9.47	3.55	0.69	0.379
Tamolitch (11)										
Min	49.77	1.459	16.99	9.07	0.158	7.95	9.32	3.14	0.62	0.324
Mean	50.03	1.502	17.12	9.32	0.161	8.14	9.49	3.24	0.65	0.336
Max	50.37	1.541	17.24	9.46	0.163	8.50	9.64	3.36	0.68	0.361
Range	0.59	0.083	0.25	0.39	0.006	0.55	0.31	0.22	0.06	0.037
Stdev	0.20	0.021	0.08	0.11	0.002	0.17	0.09	0.07	0.02	0.012
Instrument error (2σ)	0.19	0.012	0.08	0.18	0.002	0.073	0.04	0.04	0.02	0.003

Note: Major elements are normalized on a volatile-free basis; total Fe is expressed as FeO. *N*—number of rock analysis attributed to the unit and may include duplicate beads (see Tables DR1 and DR2 [text footnote 1]). Min—minimum; max—maximum; Stdev—standard deviation.

*Results of analyses for units with three or fewer samples are provided in lieu of a summary.

lain by Old Wagon Road lavas. We suspect that it is the oldest of all the units.

South of the Sand Mountain volcanic field and Carmen Reservoir, Tamolitch lavas fill the McKenzie River valley, and Tamolitch Pool emerges from beneath Tamolitch lavas. Tamolitch lavas underlie Clear Lake South and Clear Lake East lavas. Initially, we considered the Inaccessible cones to be the most likely source, but samples from these cones have compositions that match neither the Tamolitch nor Belknap lavas. Belknap lavas overlie Tamolitch and Clear Lake South lavas, and, according to Sherrod et al. (2004), also overlie Clear Lake East lavas, consistent with their young age.

Volume Estimates

Sand Mountain volcanic field lavas and scoria cones represent a DRE volume of at least 0.9 km^3; reconstructed lava flow extents suggest a DRE volume of 1.2 km^3 (Table 7). The reconstructed Sand group is the most voluminous (0.64 DRE km^3), followed by the Lost Lake (0.30 DRE km^3) and Nash (0.22 DRE km^3) groups. There is no systematic increase or decrease in unit DRE over Sand Mountain volcanic field emplacement.

DISCUSSION

In this section, we first discuss the sequence of Holocene volcanic activity in the upper McKenzie River catchment, focusing on the Sand Mountain volcanic field cluster. We then examine geochemical trends, and we show that, despite evidence that the three Sand Mountain volcanic field groups were emplaced over only a few decades, at least two, likely three, different magma sources were tapped. We then discuss evidence for vent reoccupation and migration, review the "volcanic field" designation for the Sand Mountain volcanic field, and use our findings to assess possible hazards of central Oregon Cascades volcanism.

Sequence of Eruptive Activity

The oldest mapped unit is the Tamolitch lava south of the Sand Mountain volcanic field, which entered the McKenzie River valley south of present-day Carmen Reservoir. This lava was erroneously mapped by Taylor (1965) and Sherrod et al. (2004) as late-stage Belknap lava; instead, we determined that it underlies young Belknap lava and suspect it is considerably older. This assessment was confirmed by comparison with geomagnetic secular variations for the Holocene of the western United States (Hagstrum and Champion, 2002). Although remanent directions from sites at other western U.S. volcanoes compare adequately to Tamolitch at ca. 4300, ca. 7400, and ca. 10,130 ^{14}C yr B.P., the best direct comparison is to sites in lavas erupted from the Newberry volcano northwest rift zone at ca. 7 ka (Mckay et al., 2009). We thus attribute an age of ca. 7 ka to the Tamolitch unit.

On the basis of paleomagnetic data, Sand Mountain volcanic field units were emplaced

within no more than a few decades; cosmogenic and ^{14}C ages indicate the eruptions occurred at ca. 3 ka. Cosmogenic dates for the oldest and youngest lava units (Cold Water Cove and Clear Lake East lavas, respectively) yield ages of ca. 2.9 ka. A short eruptive time scale was confirmed by examination of intermediate units, which have similar cosmogenic dates. We do not consider the anomalous 7.4 ka sample age from Clear Lake South lavas, as it is stratigraphically implausible.

SnoPark lavas have no associated vent but underlie the Nash group and the Lost Lake unit. Interestingly, the geochemical composition of tephra at the base of the Sand Mountain volcanic field tephra fall deposit is most similar to SnoPark lavas (Mckay, 2012), which suggests that the SnoPark unit was emplaced at the start of either Sand Mountain volcanic field volcanism or Sand Mountain volcanic field explosive activity. The remainder of the tephra deposit is similar to Lost Lake, Sand, and Nash group compositions, although direct comparisons are challenging because tephra compositions were based on glass analyses, and our compositional data are whole-rock analyses.

Stratigraphically, the Lost Lake group (Cold Water Cove, Fish Lake, Old Wagon Road, and Lost Lake units) appears to be the oldest of the Sand Mountain volcanic field (Fig. 6); spatially, this group extends at minimum from Clear Lake to Lost Lake. Within the Lost Lake group, the Fish Lake unit preceded the Lost Lake unit; we were unable to establish other intergroup stratigraphic relationships (Fig. 6). However, because the Cold Water Cove unit is an orphan lava, indicating that its source has either been buried or reoccupied, we hypothesize that Cold Water Cove lavas are the oldest of the Lost Lake group.

Although both the Nash and Sand groups overlie the Lost Lake eruptive units, there is limited stratigraphic control between the two. Since both the Nash and Sand groups have barren and vegetated lavas (i.e., covered with Sand Mountain volcanic field tephra soils; Deligne et al., 2013), with the contact between barren and vegetated areas coincident with unit boundaries, it appears these two groups were active concurrently. Interestingly, vents associated with the Nash and Sand groups are aligned along three different trends (Fig. 6), and the alignment of Clear Lake South A vents (N11°W) is closer to that of the Nash group (N18°W) than the Sand group (N5°E). The Great Spring unit underlies the earliest Nash units, which indicates that the Nash group is younger than at least the Great Spring, Clear Lake South A, and Clear Lake South units.

We propose therefore that the Clear Lake South eruption started along multiple vents along the Sand alignment, which, at N5°E, is aligned slightly west of the Lost Lake alignment (N7°E). This misalignment suggests that a syneruptive change in the stress field may have allowed the Clear Lake South A vents to open to the north and along a more northwestern alignment (N11°W). Subsequent emplacement of the Great Spring unit resulted in the northern end of the Sand group alignment intersecting the southern end of the Lost Lake group alignment (Fig. 6). Activity in the northern Sand group (Great Spring unit) was followed by volcanism further to the north, in the form of Early Nash I and II, which most likely erupted from vents (now buried or subsequently reoccupied) along the N18°W Nash alignment. The Ice Cap unit erupted along the southern Sand alignment before, during, or slightly after the Great Spring and/or Early Nash I and II units; in the next section, we use geochemical trends to argue that the

TABLE 4. ERUPTIVE UNIT RANGE OF TRACE-ELEMENT CONCENTRATIONS (PPM)

Eruptive unit (*N*) / Metric	Ni	Cr	Sc	V	Ba	Rb	Sr	Zr	Y	Nb	Ga	Cu	Zn	Pb	La	Ce	Th	Nd	U
NASH GROUP																			
Little Nash (16)																			
Min	125	115	20	174	348	8	736	161	22	10.8	19	38	90	2	15	39	0	23	0
Mean	132	122	21	177	354	10	752	166	24	12.1	20	56	93	5	19	43	1	25	1
Max	148	131	21	181	360	10	764	170	25	13.2	20	62	96	7	21	50	2	27	2
Range	23	16	2	7	12	2	27	8	3	2.4	2	24	6	4	6	11	3	4	2
Stdev	6	5	1	2	3	1	7	3	1	0.7	1	6	2	1	2	3	1	1	1
Nash (38)																			
Min	102	101	20	168	342	8	733	151	21	9.1	18	47	87	3	14	36	0	21	0
Mean	111	108	21	177	351	10	819	166	23	11.7	20	56	91	4	18	44	2	25	1
Max	127	117	22	181	365	11	875	175	25	13.1	22	64	95	7	22	48	3	28	2
Range	25	16	3	13	23	3	142	24	4	4.0	4	17	8	4	8	12	3	7	2
Stdev	6	3	1	2	5	1	37	6	1	0.8	1	3	2	1	2	3	1	1	1
Early Nash II (8)																			
Min	77	80	19	165	326	8	989	148	19	9.2	19	46	82	4	16	37	0	21	0
Mean	85	98	20	171	334	9	1011	152	21	10.4	20	57	84	5	19	41	2	23	1
Max	92	111	21	177	340	9	1031	156	22	11.4	21	65	86	6	21	47	3	26	1
Range	15	31	2	12	14	1	42	8	3	2.2	2	19	4	2	5	10	3	5	1
Stdev	4	10	1	4	5	0	13	3	1	0.7	1	6	1	1	2	3	1	2	0
Early Nash I (13)																			
Min	86	99	20	170	330	7	898	148	20	8.6	19	53	84	3	15	36	0	22	0
Mean	91	106	21	176	338	9	940	154	21	10.6	20	59	86	4	18	42	2	24	1
Max	99	110	22	182	346	10	992	161	23	11.7	21	63	89	7	20	45	3	26	2
Range	13	11	3	12	16	3	94	13	3	3.1	2	10	5	4	5	9	3	4	2
Stdev	3	3	1	3	5	1	33	4	1	0.8	1	3	1	1	2	3	1	1	1
SAND GROUP																			
Clear Lake East (40)																			
Min	71	112	21	168	332	7	1018	147	20	9.2	19	35	80	3	17	41	0	22	0
Mean	79	132	23	175	353	9	1075	158	22	11.2	20	59	84	5	21	48	1	26	1
Max	87	161	24	179	374	11	1093	168	24	12.4	22	64	87	7	25	54	3	30	3
Range	16	49	3	11	43	3	75	21	4	3.2	3	29	7	4	8	13	3	8	3
Stdev	4	13	1	3	9	1	15	5	1	0.7	1	4	2	1	2	3	1	2	1
Great Spring (33)																			
Min	64	121	23	177	380	8	1004	146	21	9.0	18	24	80	3	18	42	0	23	0
Mean	85	166	25	186	399	10	1036	156	23	11.7	19	60	83	5	21	48	1	27	1
Max	107	208	27	197	411	12	1079	165	25	13.1	21	81	87	7	24	54	3	30	2
Range	43	88	4	21	31	4	75	19	4	4.1	4	57	7	4	7	12	3	7	2
Stdev	12	27	1	6	9	1	17	5	1	1.1	1	9	2	1	2	3	1	1	1
Ice Cap (36)																			
Min	57	129	26	184	385	8	980	142	22	10.2	17	50	76	3	15	40	0	22	0
Mean	82	171	28	197	400	10	1024	150	24	12.6	18	62	80	5	20	45	1	26	1
Max	102	203	29	207	418	12	1048	157	26	14.7	20	68	85	7	24	52	3	29	3
Range	45	74	3	23	33	4	68	15	4	4.5	4	18	9	4	9	12	3	7	3
Stdev	15	26	1	4	7	1	16	4	1	1.2	1	3	2	1	2	3	1	2	1
Clear Lake South A (3)*																			
RC03–49	63	139	28	201	394	11	969	156	26	13.6	17	26	83	4	22	48	2	26	
RC03–50	70	154	29	205	378	11	918	156	26	13.9	20	64	81	31	21	51	2	27	
RC04–25	70	154	28	205	379	10	888	145	23	13.6	18	63	76	5	21	46	2	27	
Clear Lake South (55)																			
Min	76	167	25	182	269	9	775	141	21	12.2	16	43	77	2	14	37	0	21	0
Mean	126	240	27	200	296	11	850	151	24	14.8	18	60	82	6	18	43	2	24	1
Max	150	280	28	208	351	12	932	159	26	16.3	21	80	186	154	22	53	3	29	3
Range	74	113	3	26	82	3	157	18	4	4.1	5	38	110	152	8	16	3	8	3
Stdev	15	21	1	4	25	1	46	3	1	1.2	1	5	14	20	2	3	1	2	1

(*continued*)

TABLE 4. ERUPTIVE UNIT RANGE OF TRACE-ELEMENT CONCENTRATIONS (PPM) (*continued*)

Eruptive unit (*N*) Metric	Ni	Cr	Sc	V	Ba	Rb	Sr	Zr	Y	Nb	Ga	Cu	Zn	Pb	La	Ce	Th	Nd	U
LOST LAKE GROUP																			
Lost Lake (24)																			
Min	170	323	25	181	317	8	626	119	21	7.0	15	43	76	2	12	26	0	20	0
Mean	182	348	27	201	352	10	689	135	24	10.6	17	63	80	4	15	35	2	22	1
Max	205	394	28	211	383	11	734	145	26	12.4	19	78	84	12	18	41	3	26	2
Range	34	71	3	29	66	2	108	26	5	5.4	3	35	8	10	7	15	3	6	2
Stdev	9	19	1	7	20	1	26	7	1	1.2	1	6	2	2	2	3	1	1	1
Old Wagon Road (10)																			
Min	135	273	25	183	264	8	718	135	21	10.2	17	56	78	3	13	28	0	19	0
Mean	142	282	27	194	273	9	739	145	23	11.2	18	60	80	4	16	38	1	21	1
Max	162	310	27	199	279	10	763	152	25	13.0	19	64	82	6	18	43	2	24	2
Range	27	37	2	16	15	2	45	17	4	2.8	2	8	5	3	5	15	3	5	2
Stdev	8	11	1	5	5	1	15	5	1	0.9	1	2	1	1	2	4	1	2	1
Fish Lake (21)																			
Min	167	311	24	188	243	8	570	129	22	9.9	16	48	77	2	12	28	0	19	0
Mean	179	325	27	199	270	9	615	140	24	11.5	17	61	80	3	15	35	1	21	1
Max	186	346	28	204	316	11	698	148	25	13.0	19	65	83	7	18	44	3	23	2
Range	19	35	4	16	73	3	128	19	3	3.1	3	17	6	5	6	16	3	4	2
Stdev	4	7	1	4	21	1	28	4	1	0.8	1	4	2	1	2	4	1	1	1
Cold Water Cove (11)																			
Min	139	269	26	188	283	8	692	134	24	8.9	16	44	79	2	13	33	0	20	0
Mean	148	279	27	194	310	9	727	142	25	10.4	18	58	81	3	16	37	1	23	1
Max	159	288	28	202	328	10	765	149	26	12.0	20	64	84	4	18	41	3	25	3
Range	20	19	2	14	45	2	73	15	2	3.1	4	20	5	2	5	8	3	5	3
Stdev	6	6	1	4	18	1	26	4	1	1.1	1	6	1	0	2	3	1	1	1
OTHER SAND MOUNTAIN VOLCANIC FIELD																			
SnoPark (3)*																			
RC03–57	185	313	25	157	499	10	884	168	28	10.3	18	47	89	5	21	50	3	27	
RC11–11	187	308	24	183	509	11	925	169	26	12.4	17	59	93	4	20	47	2	28	1
RC12–08	195	316	24	197	525	11	944	172	27	11.8	18	59	93	3	18	49	3	28	1
Jack Pine (2)*																			
RC04–34	201	352	24	191	1081	18	1343	193	22	7.9	19	67	91	6	37	84	4	49	
RC12–06	193	345	25	197	1036	18	1422	211	25	11.6	20	59	95	7	34	87	4	46	1
OTHER																			
Belknap (17)																			
Min	169	284	24	174	206	10	464	129	24	12.0	17	59	77	1	9	28	0	16	0
Mean	179	299	25	192	249	11	493	133	24	12.7	18	67	82	3	14	30	1	18	1
Max	190	313	26	196	270	13	507	139	25	14.9	19	76	84	4	23	36	2	20	2
Range	21	29	2	22	64	3	43	10	2	2.9	3	17	7	3	14	8	2	4	2
Stdev	5	7	1	5	14	1	14	3	1	0.7	1	4	2	1	3	2	1	1	0
Inaccessible cones (3)*																			
SHE95-TFJ23	141	257	30	205	247	7	448	109	22	9.1	18	54	76	1	0	16	1		
SHE95-TFJ24	142	253	28	201	244	8	456	113	21	8.3	21	55	80	0	0	34	1		
SHE95-TFJ25	136	247	28	202	239	6	450	106	21	8.2	21	51	80	1	14	25	0		
Undifferentiated Belknap (3)*																			
NID10–26MK	155	253	21	161	332	20	474	138	23	11.2	18	59	79	5	16	33	3	17	0
NID10–27MK	90	164	29	229	268	10	495	154	27	13.8	19	62	84	3	14	33	2	20	1
NID10–29MK	88	170	29	222	246	9	499	149	27	14.1	19	58	83	2	13	34	1	19	1
Tamolitch (11)																			
Min	141	278	28	211	199	9	437	126	23	13.4	17	52	76	1	10	25	1	15	0
Mean	150	290	29	221	210	10	448	131	24	14.8	18	59	80	2	14	30	1	17	1
Max	164	310	31	229	219	10	453	137	25	15.7	20	64	85	4	17	32	2	20	2
Range	23	33	3	18	20	1	16	11	2	2.3	3	12	9	3	7	7	1	5	2
Stdev	6	8	1	5	6	1	5	4	1	0.6	1	4	2	1	2	2	1	1	1
Instrument error (2σ)	4	3	2	5	12	2	5	4	1	1.2	3	7	3	3	6	8	2	4	2

Note: N—number of rock analysis attributed to the unit and may include duplicate beads (see Tables DR1 and DR2 [text footnote 1]). Min—minimum; max—maximum; Stdev—standard deviation.

*Results of analyses for units with three or fewer samples are provided in lieu of a summary.

Ice Cap unit erupted slightly before the Great Spring unit. Explosive activity then deposited tephra on emplaced lavas (and providing the soil base for future forests; Deligne et al., 2013) before eruption of the Clear Lake East lavas. At about the same time as the Clear Lake East eruption, the Nash group reactivated to produce the Nash and Little Nash units. Charcoal underneath tephra attributed by previous workers to Nash and Little Nash has been dated to 2687 ± 353 cal yr B.P. (Table 1; Sherrod et al., 2004), although only the upper bound is within the time constraints permitted by the ca. 3 ka paleomagnetic ages presented in this study.

The last lava to erupt in the upper McKenzie River catchment was the Belknap lava at ca. 1.5 ka (Table 1). Belknap lava entered the McKenzie River valley but did not reach the river.

The results presented in this study and recent tephrochronology (Mckay, 2012) are inconsistent with many ^{14}C dates collected 30–50 yr ago (e.g., Chatters, 1968), dates that typically were derived from charcoal mixed in soil collected at the base of a lava unit or tephra layer. For example, the Jack Pine vent was assigned a ^{14}C date of 2265 ± 79 cal yr B.P. (Chatters, 1968; Table 1) based on charcoal found beneath Jack Pine scoria; this date would imply that the Jack Pine cone is one of the youngest units in the region. Although it is postglacial (i.e., Holocene), it is clearly surrounded by Old Wagon Road lavas (Lost Lake group). It is also compositionally distinct from other Sand Mountain volcanic field lavas. We thus suggest that contrary to Chatters's (1968) ^{14}C date, the Jack Pine cone predates the Lost Lake group and consequently the rest of the Sand Mountain volcanic field. Similar ^{14}C age contradictions exist for Fish Lake lavas (Table 1). We suggest, however, that our combined use of paleomagnetic and cosmogenic exposure age dating firmly places eruption of the main Sand Mountain volcanic field at ca. 3 ka, and that the Sand Mountain volcanic field is bracketed by older eruptions of the Jack Pine and Tamolitch (ca. 7 ka) units and younger Belknap eruptions (ca. 1.5 ka).

Geochemical Trends

We used geochemical data primarily as a mapping aid; for this reason, we do not provide a detailed analysis of the geochemical data of the Sand Mountain volcanic field; indeed, definite conclusions would require isotope data, which we did not collect. However, the geochemistry provides interesting insights into the magma tapped to form the Sand Mountain volcanic field, and it has important implications for future episodes of mafic volcanism in the central Oregon Cascades. Critically, despite the short eruptive time frame, Sand Mountain volcanic field units could not have been derived from a single upper-crustal magma reservoir. Whether the geochemical variability reflects different mantle sources, or different fractionation-assimilation-equilibration paths in the crust, is beyond the scope of this paper. We note, however, that a recent study found that the Sand Mountain lavas are isotopically heterogeneous (Mitchell and Asmerom, 2011).

Not surprisingly, lavas from Tamolitch (unknown source), Belknap, and Inaccessible cones are geochemically distinct from units within the Sand Mountain volcanic field. These

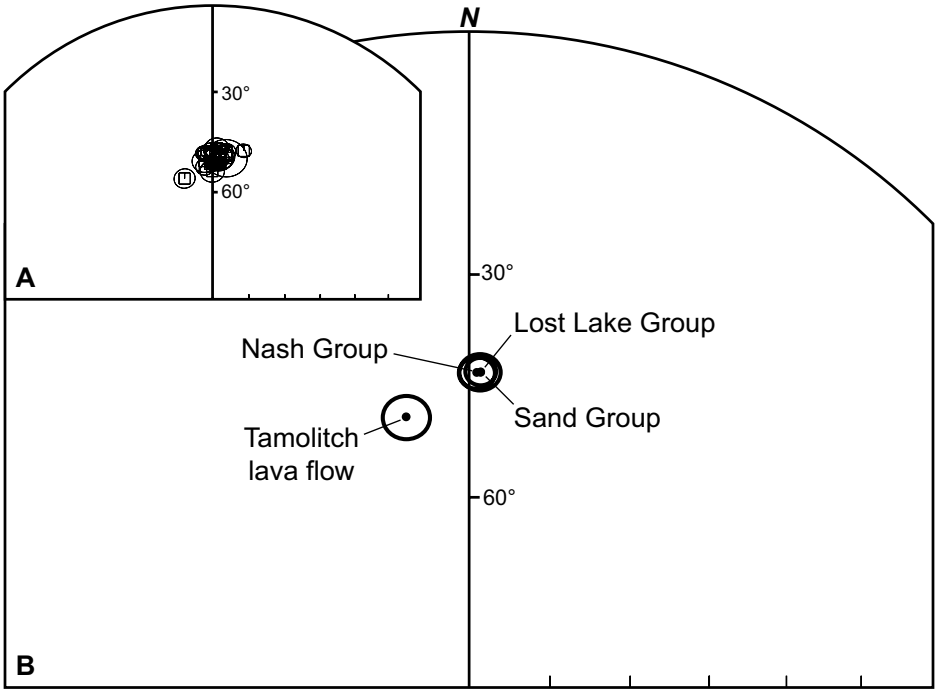

Figure 4. Part of a lower-hemisphere equal-area projection showing (A) site mean directions of remanent magnetization and ovals of 95% confidence from paleomagnetic sites sampled within the Sand Mountain volcanic field, and (B) mean remanent directions and ovals of 95% confidence for the Sand, Nash, and Lost Lake eruptive groups, compared to the site mean for the Tamolitch lava unit.

southern units are more mafic and have low Sr concentrations (Fig. 3). In this sense, they resemble lavas erupted from North Sister volcano (e.g., Schmidt and Grunder, 2009), which lies south of Belknap volcano.

Within the Sand Mountain volcanic field, the Nash group is the most distinctive. At 52.5–54 wt% SiO_2, it has, overall, the most silicic compositions in the Sand Mountain volcanic field. The units are anomalous in their low CaO and low TiO_2, as well as the inverse relationship between TiO_2 and Sr (and also Ba and Sr; Fig. 3). More curious is the enrichment in Ni relative to Cr when compared with MgO (Tables 3 and 4). This Ni enrichment precludes a common parent magma with the rest of the Sand Mountain volcanic field, as neither fractional crystallization nor crustal assimilation can cause simultaneous enrichment in Ni and SiO_2; indeed, it is not possible to have two different trends of Ni versus MgO by fractional crystallization of a single parent magma (Hart and Davis, 1978). Thus, we infer that the Nash group must have come from a different source than the rest of the Sand Mountain volcanic field. The Nash group also has a different vent alignment than the rest of the field (Fig. 6).

The Lost Lake and Sand groups appear closely related. The fact that the Lost Lake group, which erupted first, is more primitive than the Sand group suggests a trend of magma evolution with time. Within the Sand group, the Clear Lake South eruptive unit has unusually high TiO_2 and is one of the most heterogeneous units in the field, which may reflect a more complicated mixing and/or assimilation history than seen in the rest of the group. The two units sandwiched between the Clear Lake South (below) and Clear Lake East (above) eruptive units, Ice Cap and Great Spring, are very similar; the Great Spring unit transitional is between the Ice Cap and Clear Lake East eruptive units in both TiO_2 and CaO concentration. From this trend, we suggest that the Ice Cap unit erupted before the Great Spring unit. Overall, geochemical trends in the Sand group could be explained by eruption from a single magma body, but one that became more evolved with time, and may be related to magma of the Lost Lake group. Interestingly, the two groups have close vent alignments, with vents aligned N7°E in the Lost Lake group and N5°E in the Sand group; the alignments intersect beneath present-day Sand Mountain.

The presence of plagioclase microphenocrysts in Clear Lake East lavas suggests that either the magma stalled for a short time (days to a few weeks) en route to the surface and/or ascended more slowly than earlier magmas (e.g., Erlund et al., 2010). Despite having the highest crystal concentration, Clear Lake East lavas are not unusually enriched in compatible major and/or trace elements, suggesting the crystals grew in the magma rather than being entrained.

The Jack Pine cone in the northern Sand Mountain volcanic field has a very distinctive geochemical signature: It is an absarokite. Absarokites are rare in the Cascades, and this points to a unique mafic magma source that cannot be related to calc-alkaline basalts via either fractional crystallization or crustal assimilation (Bacon, 1990; Bacon et al., 1997; Conrey et al., 1997). Schmidt et al. (2008) showed that absarokites are limited to the Cascades forearc, and within the Central segment (spanning the Sand Mountain volcanic field); this composition may have originated from old metasomatized mantle, consistent with the elevated Sr and Ba concentrations (Bacon et al., 1997). Additionally, the high Ba/Nb ratio (~137, compared with <21 for the Sand Mountain volcanic field) of the Jack Pine samples suggests a strong arc-like signature (Pearce and Parkinson, 1993). From this, we conclude that although the Jack Pine cone is postglacial (i.e., Holocene), it tapped a very different source than the rest of the Sand Mountain volcanic field.

Regional Context

The Cascade arc is remarkable for the geochemical heterogeneity of erupted mafic lavas, which cannot all be related by fractional crystallization or crustal assimilation of a common melt (Bacon, 1990; Leeman et al., 1990; Bacon et al., 1997; Conrey et al., 1997). Mafic compositions include mid-ocean-ridge basalt (MORB)–like, low-K tholeiite, within-plate basalt, and a range of calc-alkaline basalt from medium-K to high-K to shoshonite and absarokite. The Cascades are also typified by eruptions derived from a variety of mafic sources within a limited space and time. Single eruptions commonly sample only one magma type, although there are exceptions (e.g., Clynne and Muffler, 2010; Deardorff and Cashman, 2012). Here, we have shown that the Sand Mountain volcanic field eruptive episode may have tapped several mafic magma sources over very short times and distances.

Regionally, extension related to the High Cascades graben is associated with considerable mafic activity in the central Oregon Cascades (Schmidt et al., 2008). North Sister volcano, located just south of the area shown in Figure 1C, was a center of mafic volcanism in the central Oregon Cascades over ~400 k.y. (Schmidt and Grunder, 2009). North Sister

TABLE 5. PALEOMAGNETIC DATA FOR THE SAND MOUNTAIN VOLCANIC FIELD AND THE TAMOLITCH LAVA UNIT

Eruptive unit	Site	XRF sample	Latitude (°N)	Longitude (°E)*	*N*/*No*	Exp. (mT)	I (°)	D (°)	α95	*k*	*R*	Plat. (°N)	Plong. (°E)
NASH GROUP													
GROUP AVERAGE			44.42	238.03	7/7		50.3	1.4	2.1	840	6.99286	76.6	53.0
Little Nash													
	LNCO Site 1	RC02-22	44.431	238.031	6/6	NRM†	49.6	3.0	3.8	318	5.98428	75.8	47.6
	LNCO Sites 2,3,4	RC02-23	44.431	238.036	17/17	NRM†	50.5	2.8	1.9	363	16.95587	76.6	47.6
			44.431	238.034	2/2		50.1	2.9	2.0	15888	1.99994	76.2	47.5
Nash													
	221B2	RC95-02	44.401	237.999	8/8	10	51.8	2.7	1.9	881	7.99206	77.9	46.9
	178B2	RC95-13	44.422	238.045	8/8	20+	48.2	359.2	2.5	511	7.98631	74.8	60.6
	FsLO 3+4	RC02-20	44.414	237.998	1212	NRM†	49.2	5.5	2.0	455	11.97583	75.1	39.3
	146B2	RC02-26	44.416	238.045	8/8	10	48.7	356.6	2.2	648	7.98919	75.0	69.6
			44.41	238.02	4/4		49.5	1.0	3.4	725	3.99586	75.9	54.6
Early Nash II													
	4371B	RC11-10	44.431	238.041	7/9	Li§	54.0	359.8	3.2	360	6.9833	80.1	59.0
SAND GROUP													
GROUP AVERAGE			44.38	238.02	8/9		50.2	2.0	2.4	521	7.98657	76.5	50.7
Clear Lake East													
	170B2#	RC02-29	44.380	238.086	8/8	30	43.4	0.1	3.9	207	7.96624	71.0	57.8
	210B2	RC02-32	44.370	238.010	10/11	20	51.0	356.7	3.3	217	9.95853	77.0	70.8
Great Spring													
	194B2	RC95-16	44.398	238.046	8/8	10+	48.2	3.0	1.9	816	7.99142	74.6	48.3
	186B2	RC95-17	44.387	238.032	8/8	20	51.9	0.4	2.1	705	7.99007	78.1	56.2
	154B2	RC02-27A	44.406	238.046	8/8	20	48.8	357.5	2.4	540	7.98704	75.2	66.6
	162B2	RC02-27B	44.406	238.046	8/8	10+	50.2	2.5	3.7	226	7.96908	76.4	49.1
			44.40	238.043	4/4		49.8	0.9	2.6	1224	3.99755	76.2	55.0
Ice Cap													
	202B2	RC02-31	44.343	238.004	8/8	10	51.7	3.1	1.6	1183	7.99408	77.8	45.8
Clear Lake South													
	CrLO 1+2	RC02-30	44.349	238.006	12/12	10	51.6	0.2	2.0	464	11.97631	77.9	57.3
	CrLO 3+4	RC95-20	44.355	238.006	12/12	10+	47.1	11.8	2.0	453	11.97572	71.4	23.8
			44.352	238.006	2/2		49.5	6.3	19.3	170	1.99413	75.1	36.5
LOST LAKE GROUP													
GROUP AVERAGE			44.42	238.03	8/8		50.1	2.1	1.8	968	7.99277	76.3	50.4
Lost Lake													
	LsLO Site 1	RCNSH-5**	44.432	238.074	12/12	NRM†	48.1	5.4	2.4	336	11.96724	74.1	40.7
	LsLO Site 2+3	RC02-24	44.435	238.063	12/12	NRM†	50.3	3.0	1.6	697	11.98423	76.4	47.0
			44.434	238.069	2/2		49.2	4.2	5.9	1799	1.99944	75.3	43.5
Old Wagon Road													
	137B2	RC02-25	44.413	238.073	9/9	20	47.3	1.6	3.1	284	8.97187	74.0	52.9
Fish Lake													
	HkmO	RC95-01	44.400	237.996	12/12	NRM†	50.3	2.6	2.6	1323	11.99168	76.5	48.6
	229B2	RC00-56	44.441	238.007	7/8	20	50.0	5.4	5.5	120	6.94985	75.7	38.9
	LvLO	RC02-21	44.428	238.017	12/12	NRM†	49.7	2.7	1.4	1000	11.98899	75.9	48.4
	FsLO 1+2	RC02-42	44.402	237.998	12/12	NRM†	52.7	356.6	2.4	327	11.96641	78.6	72.4
			44.42	238.00	4/4		50.7	1.9	3.1	901	3.99667	76.9	50.8
Cold Water Cove													
	4291B	NID11-05MK	44.362	238.013	7/8	Li§	51.9	359.0	1.6	1386	6.9957	78.1	62.1
OTHER													
Tamolitch													
	4211B	NID11-04MK	44.303	237.969	7/8	Li§	55.2	346.9	2.8	474	6.9874	76.8	111.8

Note: We use the following abbreviations: *N*/*No*—number of cores used compared to the number of original cores collected at the site, Exp. —strength of the peak alternating field used in demagnetization in milliteslas, I—remanent inclination of the site mean direction; D—remanent declination of the site mean direction, α95—95% confidence limit for the mean direction, *k*—estimate of the Fisher precision parameter, *R*—length of the resulting vector, and Plat/Plong—location in degrees north and east of the virtual geomagnetic pole calculated from the mean direction of the site.

*We follow paleomagnetic convention (McElhinney, 1973) in reporting longitude in degrees east. Obtain degrees west by subtracting the listed degrees east from 360°, e.g., the Nash Group average longitude is 121.93°W.

†NRM—no required demagnetization.

§Li—a vector component lines analysis was used.

#Site data not used to calculate Sand Mountain group mean direction.

**X-ray fluorescence (XRF) sample taken within 100 m of paleomagnetic cores.

TABLE 6. ^{3}He COSMOGENIC DATA FOR THE SAND GROUP AND COLD WATER COVE LAVA UNITS

Sample	Latitude (°N)	Longitude (°W)	Altitude* (km)	Scaling factor†	Sample mass (g)	^{3}He (cps)	^{4}He (mV)	^{3}He corr (cps§)	^{4}He corr (mV)	^{3}He (Mat/g)	^{4}He (Ta/g)	^{3}He/^{3}He (Ra#)	Age (ka)
Clear Lake East													
NID09-24	44.369	121.988	0.963	2.17	0.4189	2.6 ± 0.10	2.2 ± 0.02	2.5 ± 0.10	1.7 ± 0.16	0.66 ± 0.03	0.021 ± 0.002	136.0	2.7 ± 0.3
Ice Cap													
NID09-31	44.349	121.993	0.907	2.07	0.6610	4.0 ± 0.11	2.6 ± 0.02	3.9 ± 0.11	2.0 ± 0.17	0.64 ± 0.02	0.015 ± 0.001	31.1	2.7 ± 0.2
Clear Lake South													
RC09-44	44.347	121.996	0.860	1.99	0.4620	2.9 ± 0.09	2.8 ± 0.02	2.8 ± 0.10	2.3 ± 0.16	0.65 ± 0.02	0.025 ± 0.002	19.0	2.9 ± 0.2
NID09-19	44.355	121.993	0.917	2.09	0.3088	5.1 ± 0.06	3.4 ± 0.01	5.0 ± 0.06	2.9 ± 0.14	1.76 ± 0.03	0.047 ± 0.003	67.8	7.4 ± 0.5
NID09-29	44.360	121.991	0.932	2.11	0.7345	5.1 ± 0.13	3.2 ± 0.02	5.0 ± 0.13	2.4 ± 0.18	0.74 ± 0.02	0.017 ± 0.001	32.1	3.1 ± 0.2
NID09-30	44.359	121.990	0.938	2.13	0.8050	5.2 ± 0.06	4.3 ± 0.02	5.1 ± 0.06	2.8 ± 0.14	0.69 ± 0.01	0.017 ± 0.001	28.5	2.8 ± 0.2
Cold Water Cove													
NID09–26	44.359	121.985	0.987	2.21	0.5392	3.7 ± 0.05	2.2 ± 0.01	3.6 ± 0.05	1.7 ± 0.14	0.73 ± 0.01	0.016 ± 0.001	33.5	2.9 ± 0.2

Note: Age was determined using Licciardi et al.'s (1999) production rate (114 ± 3 g^{-1} yr^{-1}) calibrated for the Clear Lake East lava and a topographic-erosion-shielding factor of 1 (no correction); all errors are 1σ.

*Determined from light detection and ranging (LiDAR) data.

†Determined using Desilets et al. (2006).

§Counts per second.

#Ratio normalized to blank air sample.

volcano is composed of low-K calc-alkaline basaltic andesites (Schmidt and Grunder, 2009), whereas the Sand Mountain volcanic field consists of medium-K calc-alkaline basalts and basaltic andesite (Fig. 3). Finally, compared to other lavas in the High Cascade graben, the Sand Mountain volcanic field is remarkable for the relative homogeneity within single units: For example, the 1.6 ka Collier Cone lava unit on the flank of North Sister volcano has compositions ranging from andesite to dacite (Deardorff and Cashman, 2012).

Vent Alignment, Migration, and Reoccupation

The three Sand Mountain volcanic field groups erupted along a roughly N-S trend, though with slightly different vent alignments consistent with regional tectonic stresses (Taylor, 1990; Fig. 6): The Lost Lake group vents align N7°E, the Nash vents align N18°W, and the Sand vents align N5°E. The Clear Lake South A vents (N11°W) are not aligned with the Sand group to which they belong but are located and aligned between the Nash and Lost Lake groups. These differences in vent alignment suggest that each group responded to or created slightly different stress fields; perhaps earlier eruptions altered stress fields for subsequent eruptions, and a NW rotation in vent alignment occurred over the course of the Sand Mountain volcanic field eruptive episode. A simpler explanation could be that the eruptions were fed by four dikes, and each alignment corresponded to a different feeder dike. Field observations at scoria cones with exposed plumbing systems suggest that feeder dikes are no more than 100–200 m deep (e.g., Keating et al., 2008; Friese et al., 2013; Geshi and Oikawa, 2014; Harp

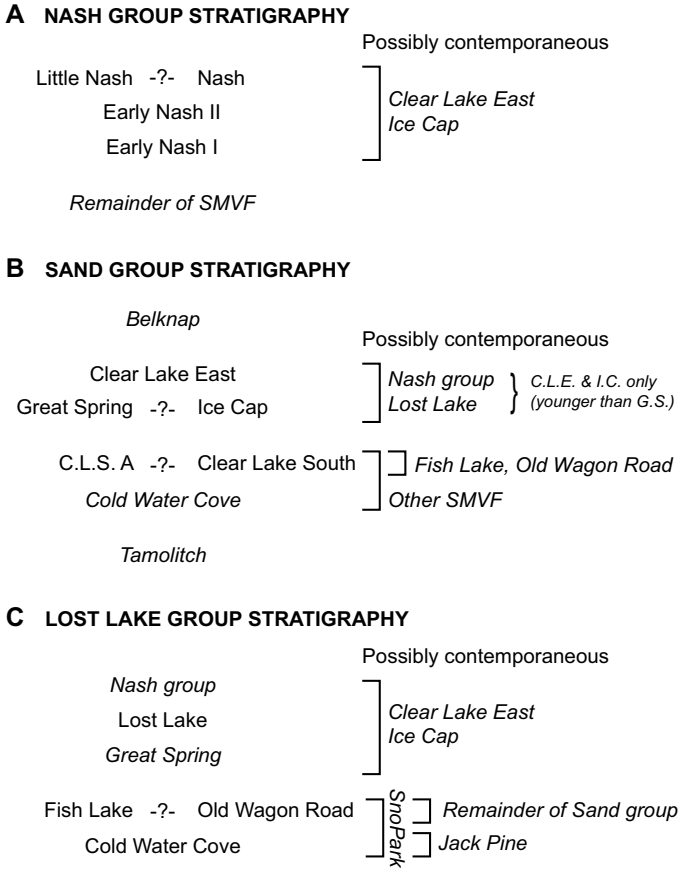

Figure 5. Stratigraphic relations within and among the (A) Nash group, (B) Sand group, and (C) Lost Lake group; units that are not part of the group are italicized. Younger units overlie older units. Units are placed side by side with a question mark (-?-) separating them if each one has similar stratigraphic relations above and below, but there is no control on which unit of the pair is older. Possibly contemporaneous units from other groups are shown on the right; brackets show the temporal range of possible overlap. SMVF—Sand Mountain volcanic field; C.L.S.A—Clear Lake South A; G.S.—Great Spring; I.C.—Ice Cap; C.L.E.—Clear Lake East.

TABLE 7. VOLUME ESTIMATES FOR SAND MOUNTAIN VOLCANIC FIELD LAVA AND SCORIA CONES

Unit*	Exposed lava (km^2)	Reconstructed lava (km^2)	Exposed lava volume* ($\times10^6$ m^3)	Reconstructed lava volume* ($\times10^6$ m^3)	Cone(s) equivalent radius† (m)	Cone(s) height (m)	Total cone(s) volume§ ($\times10^6$ m^3)	Min. vol. ($\times10^6$ m^3)	Estimated vol. ($\times10^6$ m^3)	Min. DRE# ($\times10^6$ m^3)	Estimated DRE# ($\times10^6$ m^3)
Little Nash	3.3	–	33	–	270	150	12	45	45	40	40
Nash	10.2	–	102	–	460	250	56	158	158	135	135
Early Nash II	0.8	–	8	–	–	–	–	8	>8	8	>8
Early Nash I	0.7	4.2	7	42	–	–	–	7	>42	7	>42
Clear Lake East	15.4	–	154	–	500; 100; 50; 50	240; 30; 10; 10	62	216	216	191	191
Great Spring	12.3	–	123	–	410; 330	220; 150	56	179	>179	157	>157
Ice Cap	4.9	7.9	49	79	360; 220; 70	180; 120; 30	31	80	110	67	97
Clear Lake South	8.2	19.0	82	190	200; 150; 110	100; 70; 50	7	89	197	86	194
Proto–Clear Lake South	–	–	–	–	190; 170; 150	100; 90; 40	8	8	>8	5	>5
Lost Lake	5.8	6.4	58	64	300; 210	200; 80	23	81	87	72	78
Old Wagon Road	4.1	6.6	41	67	380; 300	220; 140	46	88	113	69	94
Fish Lake	4.0	12.0	40	120	320	110	12	52	132	47	127
Cold Water Cove	0.6	–	6	–	–	–	–	6	>6	6	>6
SnoPark	0.1	–	1	–	–	–	–	1	>1	1	>1
Jack Pine	–	–	–	–	190	90	3	3	>3	2	>2
Total	*70.4*		*0.7 km^3*		*Area: 5.3 km^2*		*0.3 km^3*	*1.0 km^3*	*1.3 km^3*	*0.9 km^3*	*1.2 km^3*

*Assumed 10 m lava thickness.
†Radius of circle of equal area as cone footprint.
§Estimated for each cone using formula for volume of a cone given radius and height.
#Dense rock equivalent—assumed lava density equal to magma density,1500 kg/m^3 cone density, and 2700 kg/m^3 magma density.

and Valentine, 2015). If this were the case, then the feeder dikes for the Nash vents had to tap a different magma source than those feeding the Lost Lake and Sand vents. Additionally, several units have more than one vent, suggesting either contemporaneous activity at multiple vents or vent migration through time (Fig. 6B).

Finally, there is evidence of vent reoccupation between various groups of the Sand Mountain volcanic field. The vents of Old Wagon Road (Lost Lake group) and Great Spring (Sand group) eruptive units are in close proximity, and one of the Great Spring cones partially buries an Old Wagon Road cone (Fig. 6A). The presence of numerous orphan lavas can also be explained if vents were either buried or reoccupied; in the latter case, early vents would now be covered with cone deposits from younger eruptive units. Vent reoccupation has been observed at numerous other scoria cones, for example, in the southern Cascades (e.g., Clynne and Muffler, 2010) and during the Rangitoto eruptive episode in the Auckland volcanic field, New Zealand. In the latter, two eruptions separated by a few decades and sourced from different magma batches used the same conduit system (Needham et al., 2011). At Chagwido, Korea, two eruptions separated by ~200 k.y. appear to have occupied the same vent (Brenna et al., 2015). Similarly, Cerro Negro, Nicaragua, is a modern example of a basaltic scoria cone that has had considerable vent reoccupation: At least 22 distinct eruptions have occurred since A.D. 1850, with 1–23 yr between eruptions (McKnight and Williams, 1997).

Our detailed study of the Sand Mountain volcanic field shows that the entire "field" was erupted over as little as a few decades (and at most less than a century), tapped several magma bodies, reused vents, and shifted lava effusion locations; we suspect the latter was in response to tectonic and/or syneruptive stresses. Although our study reveals what can happen during clustered mafic volcanism, future work is needed to address (1) exactly how (and if) early activity influences the location of later activity, (2) what conditions allow several different magma sources to be first created, and then tapped, in close proximity to each other, and (3) whether the presence of numerous magma bodies in a small area produces a greater total eruptive volume (and associated "flare-up") than a single magma source.

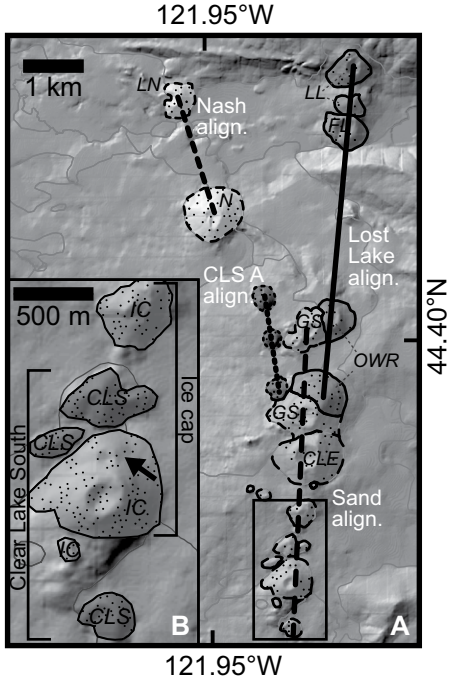

Figure 6. (A) Vent area for the entire Sand Mountain volcanic field, showing the alignment of the Lost Lake group (solid), Clear Lake South A vents (dotted), rest of Sand group (big dashes), and Nash group (small dashes). The extent of B is shown by a black rectangle. LN—Little Nash; LL—Lost Lake; FL—Fish Lake; CLS A—Clear Lake South A; GS—Great Spring; OWR—Old Wagon Road; CLE—Clear Lake East. (B) Vents of the southern Sand group (Clear Lake South [CLS] and Ice Cap [IC]). The arrow points out a small Ice Cap cone partially buried by the main Ice Cap cone. Vents are stippled and labeled by unit abbreviation (see Fig. 2).

Volcanic Field Designation

While the Sand Mountain volcanic field is an official name, it is arguably inappropriate to call it a volcanic field, given the nearby presence of numerous other Quaternary vents located within a similar tectonic setting: A volcanic field has an elevated concentration of volcanic vents often in a single tectonic setting (Valentine and Connor, 2015). Indeed, compared to other volcanic fields, such as the Michoacán-Guanajuato volcanic field in Mexico (Hasenaka and Carmichael, 1985) or the Auckland volcanic field in New Zealand (Allen and Smith, 1994), it would

be more appropriate to designate the Quaternary volcanism described in Hildreth (2007) as the "Central Oregon volcanic field," and to rename the Sand Mountain volcanic field to reflect that it has been a relatively short-lived center of volcanism within this wider volcanic field. Were this suggestion adopted, the Central Oregon volcanic field would be unusual, although not unique (see also the Michoacán-Guanajuato volcanic field), in the collocation of "monogenetic" scoria cones, shield volcanoes (Belknap, North Sister, Newberry), and complex stratovolcanoes (Three Sisters, Jefferson) in close proximity.

Local Hazard Implications for the Central Oregon Cascades

Although it is unlikely that the Sand Mountain volcanic field will reactivate, this study provides insights on possible ramifications of future mafic activity in the central Oregon Cascades, which is likely given the concentration of Holocene mafic volcanism in the area (Hildreth, 2007). For example, recent uplift observed east of South Sister volcano (Riddick and Schmidt, 2011) is only 30 km SSE of the Sand Mountain volcanic field. Although it is unlikely the South Sister uplift will lead to an eruption in the near future, the uplift has been interpreted as evidence of magma intrusion into the upper crust, consistent with this region being volcanically active.

Our study documents a cluster of mafic volcanism erupting at least 1 km^3 over no more than a few decades. Other known clusters of mafic volcanism in the Central Oregon volcanic field include the ca. 7 ka eruptions in the Newberry northwest rift zone (0.86 km^3 from 14 units, erupted over no more than a few decades; Mckay et al., 2009) and the eruptions of Collier cone, Four in One, and Yapoah on the northern flank of North Sister volcano within a few centuries of each other (Sherrod et al., 2004). Thus, similar clustered activity could be expected in the future: If a mafic eruption in a new location were to start within the Central Oregon volcanic field, responding agencies may want to consider it could be either a single short-lived event or the start of a cluster of mafic volcanism that could last a few decades.

A recent assessment of volcanic hazards in the Three Sisters region, which covers a considerable portion of the Central Oregon volcanic field, states that, in this region, the "most hazardous events at mafic volcanoes occur when rising magma interacts explosively with surface water or shallow ground water" (Scott et al., 1999, p. 7), i.e., phreatic or phreatomagmatic explosions. Overall, hazards associated with mafic volcanism in Three Sisters region are predicted to only impact areas within 10 km of the vent, and lava flows are expected to affect the greater proportion of this area. In general, the extent of Sand Mountain volcanic field lava units supports this assessment, as most Sand Mountain volcanic field lavas extend 5 km or less from their vent. Sand Mountain volcanic field lavas are also strongly influenced by topography: All Sand Mountain volcanic field vents are west of Santiam Pass (Fig. 1) on the Cascade crest, and consequently all Sand Mountain volcanic field lavas flowed west downhill. Lava flows that encountered the western High Cascade graben margin either stopped (e.g., Old Wagon Road lavas) or from there, flowed downhill into the upper McKenzie River drainage (e.g., Nash, Fish Lake, Clear Lake South, Ice Cap, and Tamolitch lavas). The topographic diversion forced by the graben margin appears to have shortened the flow length, perhaps because it forced interaction with the McKenzie River. If the river bed were dry, then the graben margin could have increased the flow length via focusing (e.g., Dietterich and Cashman, 2014). In either case, however, the primary impact of lava effusion would have been related to its effect on the McKenzie River, which was (and remains) dammed by the Clear Lake South lava; this damming would have created temporary downstream water shortages (Deligne, 2012).

Were the mafic volcanic activity to occur today in the Central Oregon volcanic field, there could be major implications for regional transportation routes if lava flows reached a highway connecting the Willamette Valley and central Oregon, particularly one of the three highways crossing the central Oregon Cascades (Santiam, McKenzie, or Willamette Passes). Given the limited number of roads in the area, however, most regional mafic volcanism is unlikely to engender significant transportation problems, although new vents within 5 km of highways could cause substantial disruptions.

We did not examine phreatomagmatism or tephra hazards associated with the Sand Mountain volcanic field. However, documentation of >2 m and 79 cm of Sand Mountain volcanic field tephra at 8 and 13 km northeast of Sand Mountain, respectively, indicates that tephra hazards associated with mafic volcanism in the central Oregon Cascades can extend further than 10 km from the vent, and the hazard can be considerably greater than currently assumed (Mckay, 2012). Finally, a certain consequence of lava inundation of forested regions would be forest fires. The rate of posteruption vegetation recovery appears to depend very much on the nature of eruptive activity; revegetation of lavas with substantial tephra coverage was much more rapid than revegetation that postdated explosive activity (Deligne et al., 2013).

CONCLUSIONS

Our study of the Sand Mountain volcanic field reveals that the 76 km^2 field was probably active for several decades, and the 13 eruptive units tapped at least two, and maybe three, different magma sources. Activity was focused at 23 or more vents. Vents that tapped the same magma body are aligned; some vent locations appear to have migrated during a single eruption and/or were reoccupied by subsequent eruptions. Distinct magma compositions were erupted from multiple aligned vents, reflecting the geometry of the underlying magma storage region. Finally, we suggest the Sand Mountain volcanic field is a misnomer and is more appropriately considered a temporal and spatial cluster of volcanism within the larger "Central Oregon volcanic field."

ACKNOWLEDGMENTS

We are indebted to Ed Taylor and Dave Sherrod for their work on the Sand Mountain volcanic field and thank them for their extensive work deciphering the central Oregon Cascades volcanic landscape. We acknowledge our field assistants: Ariana Everson, Emily Gottesfield, Kyle House, Daniele Mckay, Laureen Wagoner, and Lucy Walsh. Deligne thanks Dan Gavin, Kristina Walowski, Lucy Walsh, Kathryn Watts, and Stephanie Weaver for assistance with sample preparation and analysis. Deligne acknowledges two University of Oregon Thayer scholarships. This work benefited from conversations with Gordon Grant, Daniele Mckay, and Craig Miller. Reviews by Mike Clynne, Jan Lindsay, Greg Valentine, and Associate Editor Joselyn McPhie greatly improved the manuscript. Finally, we thank Karl Morgenstern (Eugene Water & Electric Board) and Ian Madin (Oregon Department of Geology and Mineral Industries) for light detection and ranging (LiDAR) data acquisition and access. This work was supported by National Science Foundation grants EAR-0738894 and EAR-1019848 to Cashman, who is currently supported by the AXA Research Fund and a Royal Society Wolfson Research Merit Award, and GNS Science Core Research Programme funding to Deligne. Any use of trade, firm, or product names is for descriptive purposes only and does not imply endorsement by the U.S. Government.

REFERENCES CITED

Allen, S.R., and Smith, I.E.M., 1994, Eruption styles and volcanic hazard in the Auckland volcanic field, New Zealand: Geoscience Report Shizuoka University, v. 20, p. 5–14.

Amidon, W.H., and Farley, K.A., 2011, Cosmogenic ^{3}He dating of apatite, zircon and pyroxene from Bonneville flood erosional surfaces: Quaternary Geochronology, v. 6, no. 1, p. 10–21, doi:10.1016/j.quageo.2010.03.005.

Arculus, R.J., 2003, Use and abuse of the terms calcalkaline and calcalkalic: Journal of Petrology, v. 44, no. 5, p. 929–935, doi:10.1093/petrology/44.5.929.

Bacon, C.R., 1990, Calc-alkaline, shoshonitic, and primitive tholeiitic lavas from monogenetic volcanoes near Crater Lake, Oregon: Journal of Petrology, v. 31, p. 135–166, doi:10.1093/petrology/31.1.135.

Bacon, C.R., 2008, Geologic Map of Mount Mazama and Crater Lake Caldera, Oregon: U.S. Geological Survey Scientific Investigations Map 2832, 4 sheets.

Bacon, C.R., Bruggman, P.E., Christiansen, R.L., Clynne, M.A., Donnelly-Nolan, J.M., and Hildreth, W., 1997,

Primitive magmas at five Cascade volcanic fields; melts from hot, heterogeneous sub-arc mantle: Canadian Mineralogist, v. 35, p. 397–423.

Bebbington, M., and Cronin, S.J., 2011, Spatio-temporal hazard estimation in the Auckland volcanic field, New Zealand, with a new event-order model: Bulletin of Volcanology, v. 73, no. 1, p. 55–72, doi:10.1007/s00445-010-0403-6.

Benson, G.T., 1965, The age of Clear Lake, Oregon: The Ore Bin, v. 27, p. 37–40.

Brand, B.D., Gravley, D.M., Clarke, A.B., Lindsay, J.M., Bloomberg, S.H., Agustín-Flores, J., and Németh, K., 2014, A combined field and numerical approach to understanding dilute pyroclastic density current dynamics and hazard potential: Auckland volcanic field, New Zealand: Journal of Volcanology and Geothermal Research, v. 276, p. 215–232, doi:10.1016/j.jvolgeores.2014.01.008.

Brenna, M., Cronin, S.J., Smith, I.E.M., Sohn, Y.K., and Németh, K., 2010, Mechanisms driving polymagmatic activity at a monogenetic volcano, Udo, Jeju Island, South Korea: Contributions to Mineralogy and Petrology, v. 160, no. 6, p. 931–950, doi:10.1007/s00410-010-0515-1.

Brenna, M., Németh, K., Cronin, S.J., Sohn, Y.K., Smith, I.E.M., and Wijbrans, J., 2015, Co-located monogenetic eruptions ~200 kyr apart driven by tapping vertically separated mantle source regions, Chagwido, Jeju Island, Republic of Korea: Bulletin of Volcanology, v. 77, no. 5, 43, doi:10.1007/s00445-015-0928-9.

Cebriá, J.M., Martín-Escorza, C., López-Ruiz, J., Morán-Zenteno, D.J., and Martiny, B.M., 2011, Numerical recognition of alignments in monogenetic volcanic areas: Examples from the Michoacán-Guanajuato volcanic field in Mexico and Calatrava in Spain: Journal of Volcanology and Geothermal Research, v. 201, no. 1–4, p. 73–82, doi:10.1016/j.jvolgeores.2010.07.016.

Cerling, T., 1990, Dating geomorphic surfaces using cosmogenic ^{3}He: Quaternary Research, v. 33, p. 148–156, doi:10.1016/0033-5894(90)90015-D.

Champion, D.E., 1980, Holocene Geomagnetic Secular Variation in the Western United States: U.S. Geological Survey Open-File Report 80-824, 326 p.

Chatters, R.M., 1968, Washington State University natural radiocarbon measurements I: Radiocarbon, v. 10, p. 479–498.

Clynne, M.A., and Muffler, L.J.P., 2010, Geologic Map of Lassen Volcanic National Park and Vicinity, California: U.S. Geological Survey Scientific Investigations Map 2899, scale 1:50,000, 3 sheets.

Condit, C.D., and Connor, C.B., 1996, Recurrence rates of volcanism in basaltic volcanic fields: An example from the Springerville volcanic field, Arizona: Geological Society of America Bulletin, v. 108, no. 10, p. 1225–1241, doi:10.1130/0016-7606(1996)108<1225:RROVIB>2.3.CO;2.

Conrey, R.M., Sherrod, D.R., Hooper, P.R., and Swanson, D.A., 1997, Diverse primitive magmas in the Cascade arc, northern Oregon and southern Washington: Canadian Mineralogist, v. 35, p. 367–396.

Conway, F.M., Ferrill, D.A., Hall, C.M., Morris, A.P., Stamatakos, J.A., Connor, C.B., Halliday, A.N., and Condit, C., 1997, Timing of basaltic volcanism along the Mesa Butte fault in the San Francisco volcanic field, Arizona, from ^{40}Ar/^{39}Ar dates: Implications for longevity of cinder cone alignments: Journal of Geophysical Research, v. 102, no. B1, p. 815–824, doi:10.1029/96JB02853.

Crosweller, H.S., Arora, B., Brown, S.K., Cottrell, E., Deligne, N.I., Guerrero, N.O., Hobbs, L., Kiyosugi, K., Loughlin, S.C., Lowndes, J., Nayembil, M., Siebert, L., Sparks, R.S.J., Takarada, S., and Venzke, E., 2012, Global database on large magnitude explosive volcanic eruptions (LaMEVE): Journal of Applied Volcanology, v. 1, no. 4, p. 1–13, doi:10.1186/2191-5040-1-4.

Deardorff, N.D., and Cashman, K.V., 2012, Emplacement conditions of the c. 1600 ybp Collier Cone lava flow, Oregon: A LiDar investigation: Bulletin of Volcanology, v. 74, no. 9, p. 2051–2066, doi:10.1007/s00445-012-0650-9.

Deligne, N.I., 2012, After the Flow: Landscape Response to the Emplacement of Holocene Lava Flows, Central Oregon Cascades, USA [Ph.D. thesis]: Eugene, Oregon, University of Oregon, 217 p.

Deligne, N.I., Cashman, K.V., and Roering, J.J., 2013, After the lava flow: The importance of external soil sources for plant colonization of recent lava flows in the central Oregon Cascades, USA: Geomorphology, v. 202, p. 15–32, doi:10.1016/j.geomorph.2012.12.009.

Desilets, D., Zreda, M., and Pradu, T., 2006, Extended scaling factors for in situ cosmogenic nuclides: New measurements at low latitude: Earth and Planetary Science Letters, v. 246, no. 3–4, p. 265–276, doi:10.1016/j.epsl.2006.03.051.

de Silva, S., and Lindsay, J.M., 2015, Primary volcanic landforms, *in* Sigurdsson, H., Houghton, B., McNutt, S., Rymer, H., and Stix, J., eds., The Encyclopedia of Volcanoes (2nd ed.): San Diego, California, Academic Press, p. 273–297, doi:10.1016/B978-0-12-385938-9.00015-8.

Dietterich, H.R., and Cashman, K.V., 2014, Channel networks within lava flows: Formation, evolution, and implications for flow behavior: Journal of Geophysical Research–Earth Surface, v. 119, p. 1704–1724, doi:10.1002/2014JF003103.

Erlund, E.J., Cashman, K.V., Wallace, P.J., Pioli, L., Rosi, M., Johnson, E., and Delgado Granados, H., 2010, Compositional evolution of magma from Parícutin Volcano, Mexico: The tephra record: Journal of Volcanology and Geothermal Research, v. 197, no. 1–4, p. 167–187, doi:10.1016/j.jvolgeores.2009.09.015.

Friese, N., Frithjof, A.B., Tanner, B.C., Gústafsson, L.E., and Siegesmund, S., 2013, From feeder dykes to scoria cones: The tectonically controlled plumbing system of the Rauðhólar volcanic chain, Northern volcanic zone, Iceland: Bulletin of Volcanology, v. 75, no. 6, p. 1–19, doi:10.1007/s00445–013–0717–2.

Geshi, N., and Oikawa, T., 2014, The spectrum of basaltic feeder systems from effusive lava eruption to explosive eruption at Miyakejima volcano, Japan: Bulletin of Volcanology, v. 76, p. 797, doi:10.1007/s00445-014-0797-7.

Gill, J.B., 1981, Orogenic Andesites and Plate Tectonics: Berlin, Germany, Springer-Verlag, 336 p., doi:10.1007/978-3-642-68012-0.

Guilbaud, M.-N., Siebe, C., Layer, P.W., Salinas, S., Castro-Govea, R., Garduño-Monroy, V.H., and Le Corvec, N., 2011, Geology, geochronology, and tectonic setting of the Jorullo volcano region, Michoacán, México: Journal of Volcanology and Geothermal Research, v. 201, no. 1–4, p. 97–112, doi:10.1016/j.jvolgeores.2010.09.005.

Hagstrum, J.T., and Champion, D.E., 2002, A Holocene paleosecular variation record from ^{14}C-dated volcanic rocks in western United States: Journal of Geophysical Research, v. 107, no. B1, p. EPM 8-1–EPM 8-14, doi:10.1029/2001JB000524.

Harp, A.G., and Valentine, G.A., 2015, Shallow plumbing and eruptive processes of a scoria cone built on steep terrain: Journal of Volcanology and Geothermal Research, v. 294, p. 37–55, doi:10.1016/j.jvolgeores.2015.02.008.

Hart, S.R., and Davis, K.E., 1978, Nickel partitioning between olivine and silicate melt: Earth and Planetary Science Letters, v. 40, p. 203–219, doi:10.1016/0012-821X(78)90091-2.

Hasenaka, T., and Carmichael, I.S.E., 1985, The cinder cones of Michoacán–Guanajuato, central Mexico: Their age, volume and distribution, and magma discharge rate: Journal of Volcanology and Geothermal Research, v. 25, no. 1–2, p. 105–124, doi:10.1016/0377-0273(85)90007-1.

Hildreth, W., 2007, Quaternary Magmatism in the Cascades: Geologic Perspectives: U.S. Geological Survey Professional Paper 1744, 136 p.

Keating, G.N., Valentine, G.A., Krier, D.J., and Perry, F.V., 2008, Shallow plumbing systems for small-volume basaltic volcanoes: Bulletin of Volcanology, v. 70, p. 563–582, doi:10.1007/s00445-007-0154-1.

Kereszturi, G., Csillag, G., Németh, K., Sebe, K., Balogh, K., and Jáger, V., 2010, Volcanic architecture, eruption mechanism and landform evolution of a Plio/Pleistocene intracontinental basaltic polycyclic monogenetic volcano from the Bakony-Balaton Highland volcanic field, Hungary: Open Geosciences, v. 2, no. 3, p. 362–384, doi:10.2478/v10085-010-0019-2.

Kereszturi, G., Németh, K., Csillag, G., Balogh, K., and Kovács, J., 2011, The role of external environmental factors in changing eruption styles of monogenetic volcanoes in a Mio/Pleistocene continental volcanic field in western Hungary: Journal of Volcanology and Geothermal Research, v. 201, no. 1–4, p. 227–240, doi:10.1016/j.jvolgeores.2010.08.018.

Kuntz, M.A., Champion, D.E., Spiker, E.C., and Lefebvre, R.H., 1986, Contrasting magma types and steady-state, volume-predictable, basaltic volcanism along the Great Rift, Idaho: Geological Society of America Bulletin, v. 97, no. 5, p. 579–594, doi:10.1130/0016-7606(1986)97<579:CMTASV>2.0.CO;2.

Le Bas, M.J., Le Maitre, R.W., Streckeisen, A., and Zanettin, B., 1986, A chemical classification of volcanic rocks based on the total alkali-silica diagram: Journal of Petrology, v. 27, no. 3, p. 745–750, doi:10.1093/petrology/27.3.745.

Le Corvec, N., Spörli, K.B., Rowland, J., and Lindsay, J.M., 2013a, Spatial distribution and alignments of volcanic centers: Clues to the formation of monogenetic volcanic fields: Earth-Science Reviews, v. 124, p. 96–114, doi:10.1016/j.earscirev.2013.05.005.

Le Corvec, N., Bebbington, M.S., Lindsay, J.M., and McGee, L.E., 2013b, Age, distance, and geochemical evolution within a monogenetic volcanic field: Analyzing patterns in the Auckland volcanic field eruption sequence: Geochemistry Geophysics Geosystems, v. 14, p. 3648–3665, doi:10.1002/ggge.20223.

Leeman, W.P., Smith, D., Hildreth, W., Palacz, Z., and Rogers, N., 1990, Compositional diversity of late Cenozoic basalts in a transect across the southern Washington Cascades: Implications for subduction zone magmatism: Journal of Geophysical Research, v. 95, p. 19,561–19,582, doi:10.1029/JB095iB12p19561.

Licciardi, J.M., Kurz, M.D., Clark, P.U., and Brook, E.J., 1999, Calibration of cosmogenic ^{3}He production rates from Holocene lava flows in Oregon, USA, and effects of the Earth's magnetic field: Earth and Planetary Science Letters, v. 172, p. 261–271, doi:10.1016/S0012-821X(99)00204-6.

McCaffrey, R., Qamar, A.I., King, R.W., Wells, R., Khazaradze, G., Williams, C.A., Stevens, C.W., Vollick, J.J., and Zwick, P.C., 2007, Fault locking, block rotation and crustal deformation in the Pacific Northwest: Geophysical Journal International, v. 169, no. 3, p. 1315–1340, doi:10.1111/j.1365-246X.2007.03371.x.

McElhinny, M.W., 1973, Paleomagnetism and Plate Tectonics: Cambridge, UK, Cambridge University Press, 368 p.

McGee, L.E., Millet, M.-A., Smith, I.E.M., Németh, K., and Lindsay, J.M., 2012, The inception and progression of melting in a monogenetic eruption: Motukorea Volcano, the Auckland volcanic field, New Zealand: Lithos, v. 155, p. 360–374, doi:10.1016/j.lithos.2012.09.012.

McGetchin, T.R., Settle, M., and Chouet, B.A., 1974, Cinder cone growth modeled after Northeast crater, Mount Etna, Sicily: Journal of Geophysical Research, v. 79, no. 23, p. 3257–3272, doi:10.1029/JB079i023p03257.

Mckay, D., 2012, Recent Mafic Eruptions at Newberry Volcano and in the Central Oregon Cascades: Physical Volcanology and Implications for Hazards [Ph.D. thesis]: Eugene, Oregon, University of Oregon, 146 p.

Mckay, D., Donnelly-Nolan, J.M., Jenson, R.A., and Champion, D.E., 2009, The post-Mazama northwest rift zone eruption at Newberry volcano, Oregon, *in* O'Connor, J.E., Dorsey, R.J., and Madin, I.P., eds., Volcanoes to Vineyards: Geologic Field Trips through the Dynamic Landscape of the Pacific Northwest: Geological Society of America Field Guide 15, p. 91–110, doi:10.1130/2009.fl d015(05).

McKnight, S.B., and Williams, S.N., 1997, Old cinder cone of young composite volcano?: The nature of Cerro Negro, Nicaragua: Geology, v. 25, no. 4, p. 339–342, doi:10.1130/0091-7613(1997)025<0339:OCCOYC>2.3.CO;2.

Mitchell, E.C., and Asmerom, Y., 2011, U-series isotope systematics of mafic magmas from central Oregon: Implications for fluid involvement and melting processes in

the Cascade arc: Earth and Planetary Science Letters, v. 312, p. 378–389, doi:10.1016/j.epsl.2011.09.060.

Needham, A.J., Lindsay, J.M., Smith, I.E.M., Augustinus, P., and Shane, P.A., 2011, Sequential eruption of alkaline and sub-alkaline magmas from a small monogenetic volcano in the Auckland volcanic field, New Zealand: Journal of Volcanology and Geothermal Research, v. 201, no. 1–4, p. 126–142, doi:10.1016/j.jvolgeores.2010.07.017.

Németh, K., Cronin, S.J., Smith, I.E.M., and Agustín-Flores, J., 2012, Amplified hazard of small-volume monogenetic eruptions due to environmental controls, Orakei Basin, Auckland volcanic field, New Zealand: Bulletin of Volcanology, v. 74, no. 9, p. 2121–2137, doi:10.1007/s00445-012-0653-6.

Nieland, J., 1970, "Spatter Cone Pits": Sand Mountain Lava Field, Oregon Cascades: The Ore Bin, v. 32, p. 231–236.

Pearce, J.A., and Parkinson, I.J., 1993, Trace element models for mantle melting: Application to volcanic arc petrogenesis, *in* Prichard, H.M., Alabaster, T., Harris, N.B.W., and Neary, C.R., eds., Magmatic Processes and Plate Tectonics: Geological Society of London Special Publication 76, p. 373–403, doi:10.1144/GSL.SP.1993.076.01.19.

Pioli, L., Erlund, E., Johnson, E., Cashman, K.V., Wallace, P., Rosi, M., and Delgado Granados, H., 2008, Explosive dynamics of violent Strombolian eruptions: The eruption of Parícutin volcano 1943–1952 (Mexico): Earth and Planetary Science Letters, v. 271, no. 1–4, p. 359–368, doi:10.1016/j.epsl.2008.04.026.

Rasoazanamparany, C., Widom, E., Valentine, G.A., Smith, E.I., Cortés, J.A., Kuentz, D., and Johnsen, R., 2015, Origin of chemical and isotopic heterogeneity in a mafic, monogenetic volcanic field: A case study of the Lunar Crater volcanic field, Nevada: Chemical Geology, v. 397, p. 76–93, doi:10.1016/j.chemgeo.2015.01.004.

Reimer, P.J., Baillie, M.G.L., Bard, E., Bayliss, A., Beck, J.W., Blackwell, P.G., Bronk Ramsey, C., Buck, C.E., Burr, G.S., Edwards, R.L., Friedrich, M., Grootes, P.M., Guilderson, T.P., Hajdas, I., Heaton, T.J., Hogg, A.G., Hughen, K.A., Kaiser, K.F., Kromer, B., McCormac, F.G., Manning, S.W., Reimer, R.W., Richards, D.A., Southon, J.R., Talamo, S., Turney, C.S.M., van der Plicht, J., and Weyhenmeyer, C.E., 2009, IntCal09 and Marine09 radiocarbon age calibration curves, 0–50,000 years cal BP: Radiocarbon, v. 51, p. 1111–1150.

Riddick, S., and Schmidt, D.A., 2011, Time-dependent changes in volcanic inflation rate near Three Sisters, Oregon, revealed by InSAR: Geochemistry Geophysics Geosystems, v. 12, no. 12, p. 1–14, doi:10.1029/2011GC003826.

Rowland, S.K., Jurado-Chichay, Z., Ernst, G., and Walker, G.P.L., 2009, Pyroclastic deposits and lava flows from the 1759–1774 eruption of El Jorullo, Mexico: Aspects of 'violent Strombolian' activity and comparison with Parícutin, *in* Thordarsson, T., Self, S., Larsen, G., Rowland, S.K., and Hoskuldsson, A., eds., Studies in Volcanology: The Legacy of George Walker: International Association of Volcanology and Chemistry of the Earth's Interior (IAVCEI) Special Publication 2, p. 105–128.

Schmidt, M.E., and Grunder, A.L., 2009, The evolution of North Sister, a volcano shaped by extension and ice in the central Oregon Cascade arc: Geological Society of America Bulletin, v. 121, p. 643–662, doi:10.1130/B26442.1.

Schmidt, M.E., Grunder, A.L., and Rowe, M.C., 2008, Segmentation of the Cascade arc as indicated by Sr and Nd isotopic variation among diverse primitive basalts: Earth and Planetary Science Letters, v. 266, p. 166–181, doi:10.1016/j.epsl.2007.11.013.

Scott, W.E., Iverson, R.M., Schilling, S.P., and Fisher, B.J., 1999, Volcano Hazards in the Three Sisters Region, Oregon: U.S. Geological Survey Open-File Report 99-437, 14 p.

Sherrod, D.R., and Smith, J.G., 1990, Quaternary extrusion rates of the Cascade Range, northwestern United States and southern British Columbia: Journal of Geophysical Research, v. 95, p. 465–474, doi:10.1029/JB095iB12p19465.

Sherrod, D.R., Taylor, E.M., Ferns, M.L., Scott, W.E., Conrey, R.M., and Smith, G.A., 2004, Geologic Map of the Bend 30- by 60-Minute Quadrangle, Central Oregon: U.S. Geological Survey Miscellaneous Investigations Map I-2683, scale 1:100,000, 2 sheets.

Stearns, H.T., 1929, Geology and Water Resources of the Upper McKenzie Valley, Oregon: U.S. Geological Survey Water-Supply Paper 597-D, p. 171–188.

Stuiver, M., Reimer, P.J., and Braziunas, T.F., 1998, High-precision radiocarbon age calibration for terrestrial and marine samples: Radiocarbon, v. 40, p. 1127–1151.

Stuiver, M., Reimer, P.J., and Reimer, R.W., 2005, CALIB 5.0., http://calib.qub.ac.uk/calib/ (last accessed 29 April 2016).

Taylor, E.M., 1965, Recent volcanism between Three Fingered Jack and North Sister: Oregon Cascade Range: The Ore Bin, v. 27, p. 121–147.

Taylor, E.M., 1968, Roadside Geology, Santiam and McKenzie Pass Highways, Oregon, *in* Dole, H.M., ed., Andesite Conference Guidebook: Portland, Oregon, Department of Geology and Mineral Industries, p. 3–33.

Taylor, E.M., 1990, Volcanic history and tectonic development of the central High Cascade Range, Oregon: Journal of Geophysical Research, v. 95, p. 19,611–19,622, doi:10.1029/JB095iB12p19611.

Valentine, G.A., and Connor, C.B., 2015, Basaltic volcanic fields, *in* Sigurdsson, H., Houghton, B., McNutt, S., Rymer, H., and Stix, J., eds., The Encyclopedia of Volcanoes (2nd ed.): San Diego, California, Academic Press, p. 273–297, doi:10.1016/B978-0-12-385938-9.00023-7.

Valentine, G.A., and Gregg, T.K.P., 2008, Continental basaltic volcanoes—Processes and problems: Journal of Volcanology and Geothermal Research, v. 177, p. 857–873, doi:10.1016/j.jvolgeores.2008.01.050.

Valentine, G.A., and Perry, F.M., 2007, Tectonically controlled, time-predictable basaltic volcanism from a lithospheric mantle source (central Basin and Range Province, USA): Earth and Planetary Science Letters, v. 261, no. 1–2, p. 201–216, doi:10.1016/j.epsl.2007.06.029.

Walker, G.W., and MacLeod, N.S., 1991, Geologic Map of Oregon: U.S. Geological Survey, scale 1:100,000, 2 sheets.

Wells, R.E., and McCaffrey, R., 2013, Steady rotation of the Cascade arc: Geology, v. 41, no. 9, p. 1027–1030, doi:10.1130/G34514.1.

Wells, R.E., Weaver, C.S., and Blakely, R.J., 1998, Fore-arc migration in Cascadia and its neotectonic significance: Geology, v. 26, p. 759–762, doi:10.1130/0091-7613(1998)026<0759:FAMICA>2.3.CO;2.

Williams, H., 1957, A Geologic Map of the Bend Quadrangle, and a Reconnaissance Geologic Map of the Central Portion of the High Cascade Mountains: Portland, Oregon, Oregon Department of Geology and Mineral Industries, scale 1:125,000 and 1:250,000, 2 sheets.

Wood, C., 1979, Monogenetic volcanoes of the terrestrial planets, *in* Proceedings of the 10th Lunar and Planetary Science Conference, Houston, Texas, Lunar and Planetary Institute: New York, Pergamon Press, p. 2815–2840.

Science Editor: David I. Schofield
Associate Editor: Jocelyn McPhie

Manuscript Received 11 August 2015
Revised Manuscript Received 1 March 2016
Manuscript Accepted 18 April 2016

Printed in the USA